Contrib Mineral Petrol (2006) 151: 539–557
DOI 10.1007/s00410-006-0081-8

ORIGINAL PAPER

Antonio Acosta-Vigil · David London
George B. Morgan VI

Experiments on the kinetics of partial melting of a leucogranite at 200 MPa H_2O and 690–800°C: compositional variability of melts during the onset of H_2O-saturated crustal anatexis

Received: 7 September 2005 / Accepted: 23 February 2006 / Published online: 31 March 2006
© Springer-Verlag 2006

Abstract We have experimentally investigated the kinetics of melting of an aplitic leucogranite (quartz + sodic plagioclase of $\approx Ab_{90}$ + K-feldspar + traces of biotite) at 690, 740, and 800°C, all at 200 MPa H_2O. Leucogranite cylinders, 3.5 mm in diameter and 7 mm in length, were run in the presence of excess H_2O using cold-seal pressure vessels for 11–2,925 h. At 690 and 740°C and any experimental time, and 800°C and short run times, silicate glass (melt at run conditions) occurs as interconnected films along most of the mineral boundaries and in fractures, with the predominant volume occurring along quartz/feldspars boundaries and quartz/plagioclase/K-feldspar triple junctions. Glass film thickness is roughly constant throughout a given experimental charge and increases with experimental temperature and run duration. The results indicate that H_2O-saturated partial melting of a quartzo-feldspathic protolith will produce an interconnected melt phase even at very low degrees (< 5 vol%) of partial melting. Crystal grain boundaries are therefore completely occluded with melt films even at the lowest degrees of partial melting, resulting in a change in the mechanism of mass transport through the rock from advection of aqueous vapor to diffusion through silicate melt. At 690 and 740°C the compositions of glasses are homogeneous and (at both temperatures) close to, but not on, the H_2O-saturated 200 MPa haplogranite eutectic; glass compositions do not change with run duration. At 800°C glasses are heterogeneous and plot away from the minimum, although their molar ratios ASI (= mol $Al_2O_3/CaO + Na_2O + K_2O$) and Al/Na are constant throughout the entire charge at any experimental time. Glass compositions within individual 800°C experiments form linear trends in (wt%) normative quartz–albite–orthoclase space. The linear trends are oriented perpendicular to the 200 MPa H_2O haplogranite cotectic line, reflecting nearly constant albite/orthoclase ratio versus variable quartz/feldspar ratio, and have endpoints between the 800°C isotherms on the quartz and feldspar liquidus surfaces. With increasing experimental duration the trends migrate from the potassic side of the minimum toward the bulk rock composition located on the sodic side, due to more rapid (and complete) dissolution of K-feldspar relative to plagioclase. The results indicate that partial melting at or slightly above the solidus (690–740°C) is interface reaction-controlled, and produces disequilibrium melts of near-minimum composition that persist metastably for up to at least 3 months. Relict feldspars show no change in composition or texture, and equilibration between melt and feldspars might take from a few to tens of millions of years. Partial melting at temperatures well above the solidus (800°C) produces heterogeneous, disequilibrium liquids whose compositions are determined by the diffusive transport properties of the melt and local equilibrium with neighboring mineral phases. Feldspars recrystallize and change composition rapidly. Partial melting and equilibration between liquids and feldspars might take from a few to tens of years (H_2O-saturated conditions) at these temperatures well above the solidus.

Communicated by T. L. Grove

A. Acosta-Vigil · D. London · G. B. Morgan VI
School of Geology and Geophysics, University of Oklahoma, 100 East Boyd Street, Room 810 SEC, Norman, OK 73019, USA

Present address: A. Acosta-Vigil (✉)
Departamento de Mineralogía y Petrología, Facultad de Ciencias, Universidad de Granada, Fuentenueva s/n, 18002 Granada, Spain
E-mail: aacosta@ugr.es
Tel.: +34-958-248535
Fax: +34-958-243368

Introduction

Many theoretical studies and experimental programs have provided information about the characteristics of geologic systems at equilibrium for relevant *P–T–X* geologic conditions. These important data constitute a reference frame to which the compositions of natural

rocks are often compared. However, textures and (mineral, bulk) compositions of most metamorphic and igneous rocks are the result of a number of superimposed processes that did not go to completion due to sluggish kinetics of the reactions involved. Therefore, kinetic studies in petrology dealing with the T–X–t path followed by a system on its way toward a state of equilibrium can be equally important for interpreting geological data and quantifying the rates of geological processes (e.g. Kirkpatrick 1981; Lasaga 1981; Loomis 1983; Watson 1996; Lasaga 1998). Diffusive transport properties of silicate liquids represent one key to understanding the kinetics of magma-related processes such as partial melting, magma mixing, assimilation, and crystallization (e.g. Watson 1982; Watson and Jurewicz 1984; Baker 1990; van der Laan and Wyllie 1993; Lesher 1994; Chakraborty et al. 1995; Liang et al. 1996). Although several studies have provided information about diffusion in H_2O-saturated haplogranite liquids (e.g. Watson 1982; Baker 1990, 1991; van der Laan and Wyllie 1993; Mungall et al. 1998; Acosta-Vigil et al. 2005, 2006), there remains a poor understanding of the kinetic details of how granitic melts are generated from crustal protoliths. Whereas there is some information on the distribution of melt phase during partial melting of natural crustal rocks (Mehnert et al. 1973; Büsch et al. 1974; Arzi 1978; Brearley and Rubie 1990; Hacker 1990; Rutter and Neumann 1995; Wolf and Wyllie 1995; Rushmer 1995, 1996; Sawyer 2001; Holness et al. 2005), there is very little information on the precise composition of the melt phase as a function of textural location, P–T conditions, and time (Brearley and Rubie 1990; Holness et al. 2005). We also have a poor understanding of the conditions under which restites recrystallize (Johannes 1980; Johannes and Holtz 1992) or the velocity of specific processes controlling melting rates during the major melting reactions in the continental crust. Thus, little is known about the compositions of initial melts generated in different micro-domains of a protolith, how individual liquid aliquots evolve toward a homogeneous melt phase via diffusion, the time required to attain chemical homogeneity in bulk liquid and restite-melt equilibration, and how this timeframe compares with inferred times for separation of melt from restite. These topics are crucial to determining the point at which the compositions of granite melts mirror those of their source area (e.g. ASI values, Acosta-Vigil et al. 2002, 2003) (ASI = mol $Al_2O_3/[(CaO)+(Na_2O)+(K_2O)]$), or the degree of chemical homogeneity of granite melts upon segregation and extraction from their source rocks. This study represents a step directed at gaining information on these subjects by experimentally investigating one of the simplest cases of anatexis: the H_2O-saturated melting of a leucogranite at 200 MPa in the temperature range of 690–800°C. This is actually a complex experimental problem that possesses multiple spatial variables (e.g. the size and distribution of constituent mineral grains) and time variables as reflected by the kinetics of multiphase melting and diffusion. The study presented here is a culmination of our similar melting and diffusion experiments that involved experimental configurations with fewer phases, and simpler spatial configurations and kinetic variables (Acosta-Vigil et al. 2002, 2003, 2005, 2006).

Materials and methods

Starting materials and experimental methods

The starting materials (Table 1) are cylinders that were cored from a fine-grained homogeneous granitic layer of aplite from the Little Three pegmatite, California (sample 3c of Morgan and London 1999). The aplite is equigranular, subhedral to granoblastic, with a grain size of 0.1–0.5 mm (mean of ≈0.3 mm), and comprised mostly of subequal amounts of quartz, plagioclase ($\sim Ab_{90}An_9Or_1$) and K-feldspar ($\sim Ab_9Or_{91}$), with traces (<1%) of biotite, tourmaline and muscovite, and accessory zircon, monazite and xenotime (Fig. 1). K-feldspar is homogeneous and anhedral; plagioclase is subhedral to anhedral and shows only minor zoning or recrystallization to slightly more sodic rims; quartz is subhedral to anhedral. The aplite is weakly layered in terms of variation in modal proportions of quartz to feldspars. The presence of inter- and intra-granular fractures in the starting aplite may influence the distribution of melt phase during partial melting. We studied both unreacted starting aplite cylinders and pressurized aplite cylinders (1-day runs at 200 MPa and 25°C, see Table 2) under the scanning electron microscope (SEM). In both cases we detected the presence of abundant intra-granular fractures within plagioclase and, less frequently, within K-feldspar and quartz throughout the cylinders (Fig. 1). Note also that not all contacts among grains are sealed. Hence, although some fractures may have formed upon decompression of experimental charges, some others were already present in the starting cylinders and/or have formed during the experiments prior to quenching. Cylinders ≈3.5 mm in diameter and ≈7 mm in length were cleaned with de-ionized, ultra-filtered (DIUF) water in an ultrasonic bath. The cylinders were loaded into gold capsules (I.D. of ≈3.6 mm) with variable amounts of DIUF water. Capsules were placed inside subhorizontal NIMONIC 105® cold-seal vessels, pressurized cold, and then the temperature was raised at a rate of 40°C/min. The target pressure was 200 MPa, and target temperatures were 690, 740, and 800°C (Table 2); variations from these values during the experiments were less than ±10 bars and ±3°C, respectively. Pressure was measured with a factory calibrated Heise bourdon tube gauge, and temperature was measured with an internal chromel–alumel thermocouple. Respective total pressure and temperature uncertainties are <10 MPa and ±4°C. Oxygen fugacity was controlled indirectly by the composition of the reaction vessels at ≈0.5 log units below the Ni–NiO buffer. This estimation is based on the fO_2-dependence

Table 1 Electron microprobe analyses (wt%) of starting mineral phases and whole rock (WR)

Material No. analyses	Plagioclase[b] 12	Alkali feldspar[b] 30	Biotite[b] 443	WR, LT3C-10[c] 40	WR, LT3C-20[c] 25	WR, LT3C-21[c] 25	Mean WR 90
SiO_2	65.64 (0.73)	64.36 (0.23)	34.49 (0.38)	79.79 (1.28)	80.91 (0.94)	78.92 (0.74)	79.86 (1.30)
Al_2O_3	22.10 (0.42)	19.20 (0.08)	18.76 (0.22)	11.85 (0.72)	11.31 (0.48)	12.45 (0.37)	11.87 (0.69)
TiO_2	n.d.	n.d.	1.18 (0.08)	n.d.	n.d.	n.d.	n.d.
FeO[a]	0.03 (0.03)	0.02 (0.02)	26.22 (0.78)	0.18 (0.03)	0.20 (0.04)	0.29 (0.04)	0.21 (0.05)
MnO	n.d.	n.d.	1.06 (0.06)	0.00 (0.01)	0.00 (0.01)	0.01 (0.01)	0.00 (0.01)
MgO	n.d.	n.d.	3.21 (0.09)	0.01 (0.01)	0.02 (0.01)	0.03 (0.01)	0.02 (0.01)
CaO	2.13 (0.50)	0.02 (0.01)	0.07 (0.02)	0.65 (0.10)	0.73 (0.07)	0.70 (0.07)	0.69 (0.09)
BaO	n.d.	n.d.	<0.03	0.02 (0.02)	0.02 (0.02)	0.02 (0.02)	0.02 (0.02)
Na_2O	10.62 (0.36)	0.94 (0.08)	0.09 (0.05)	4.20 (0.24)	4.14 (0.16)	4.39 (0.14)	4.23 (0.21)
K_2O	0.28 (0.07)	15.29 (0.13)	8.76 (0.14)	3.26 (0.13)	2.63 (0.09)	3.18 (0.08)	3.06 (0.28)
F	n.d.	n.d.	0.32 (0.05)	0.03 (0.04)	0.05 (0.05)	0.05 (0.04)	0.04 (0.04)
Cl	n.d.	n.d.	0.06 (0.01)	n.d.	n.d.	n.d.	n.d.
F = O			−0.14	−0.01	−0.02	−0.02	−0.02
Cl = O			−0.01				
ASI	1.021	1.059	1.923	1.019 (0.025)	1.030 (0.027)	1.045 (0.022)	1.030 (0.026)
Mg number			0.18	0.13 (0.06)	0.13 (0.06)	0.14 (0.03)	0.14 (0.05)
K number	0.02	0.91	0.99	0.34 (0.01)	0.29 (0.01)	0.32 (0.01)	0.32 (0.02)
Moles Al/Na				1.72 (0.05)	1.66 (0.06)	1.73 (0.05)	1.70 (0.06)
Moles Al/K				3.35 (0.14)	3.98 (0.16)	3.62 (0.11)	3.61 (0.30)
Norm Qtz				38.67	41.79	36.60	39.02
Norm Ab	88.6	8.6		33.25	32.58	34.44	33.34
Norm Or	1.6	91.3		18.02	14.42	17.43	16.84
Norm An	9.8	0.1		3.03	3.37	3.22	3.18
Norm Hy				0.34	0.40	0.59	0.47
Norm Crn				0.21	0.30	0.48	0.33
Norm Ab/An	9.0	86.0		10.97	9.67	10.70	10.48
Observations				1–3% Relict Qtz	1–3% Relict Qtz	<1% Relict Qtz	

[a]Total Fe as FeO
[b]From Morgan and London (1999)
[c]LT3C-# refers to experiment labels, see Table 2. Analyses are shown on an anhydrous basis

of tin solubility in H_2O-saturated haplogranite melts, which was measured by Wolf et al. (1994) and compared to data from Taylor and Wall (1992) and Linnen et al. (1996). The duration of the experiments was in the range of 11–2,925 h. Runs were quenched isobarically at a rate of 75°C/min, using a jet of compressed air and water. After quench, capsules were weighed to check for leakage, then punctured, placed in a dessicator overnight, and re-weighed to check for the presence of free water. The dried samples were mounted in Buehler Transoptic® thermal plastic, ground to the center of the cylinders, and polished to a final grit size of 0.3 μm for microprobe analysis.

Analytical methods

Minerals and glasses in the experimental runs were analyzed with a Cameca SX-50 electron microprobe at the University of Oklahoma. Matrix reduction used the PAP correction algorithm (Pouchou and Pichoir 1985). Mineral phases were analyzed using an accelerating voltage of 20 kV, a beam current of 10 nA, and a 3 μm spot size. Counting times were 30 s on peak for all elements except Ca, Ba, Sr and Fe; Ca, Ba and Sr were counted for 45 s, and Fe was counted for 60 s. Glasses were analyzed using two beam conditions as recommended by Morgan and London (1996, 2005), also with 20 kV accelerating voltage. An initial condition with 2 nA beam current was used for Na, K, Ca, Al, and Si; Na, Al, and K were analyzed first and concurrently to minimize alkali volatilization and attendant changes in elemental ratios. All other components were analyzed using a 20 nA beam current. Where possible, glasses were analyzed using a 20 μm spot size. For experiments in which glass domains were too small to accommodate a 20 μm spot, a 5 μm spot was used and Na_2O, SiO_2 and Al_2O_3 values were corrected by reference to analyses of a water-saturated glass (200 MPa H_2O minimum composition) containing ≈6.6 wt% H_2O as discussed by Morgan and London (1996, 2005). Counting times were 30 s on peak for all elements, yielding calculated 3-σ minimum detection limits of ≤ 0.02 wt% for Na_2O, K_2O and Al_2O_3, ≈0.05 wt% for SiO_2, and ≤ 0.03 wt% for all other oxides components. Based on counting statistics, analytical uncertainties relative to their reported concentrations in glass are in the range of ±0.5 to 1.0% for SiO_2 and Al_2O_3, and ±1.5 to 3.0% for Na_2O and K_2O. H_2O concentrations in glass were calculated by difference of the electron microprobe analyses totals from 100%, with an accuracy better than 10% relative (Morgan and London 1996, 2005; Acosta-Vigil et al. 2003). The maximum uncertainty for the reported ASI values is ±0.035, calculated by the propagation of errors.

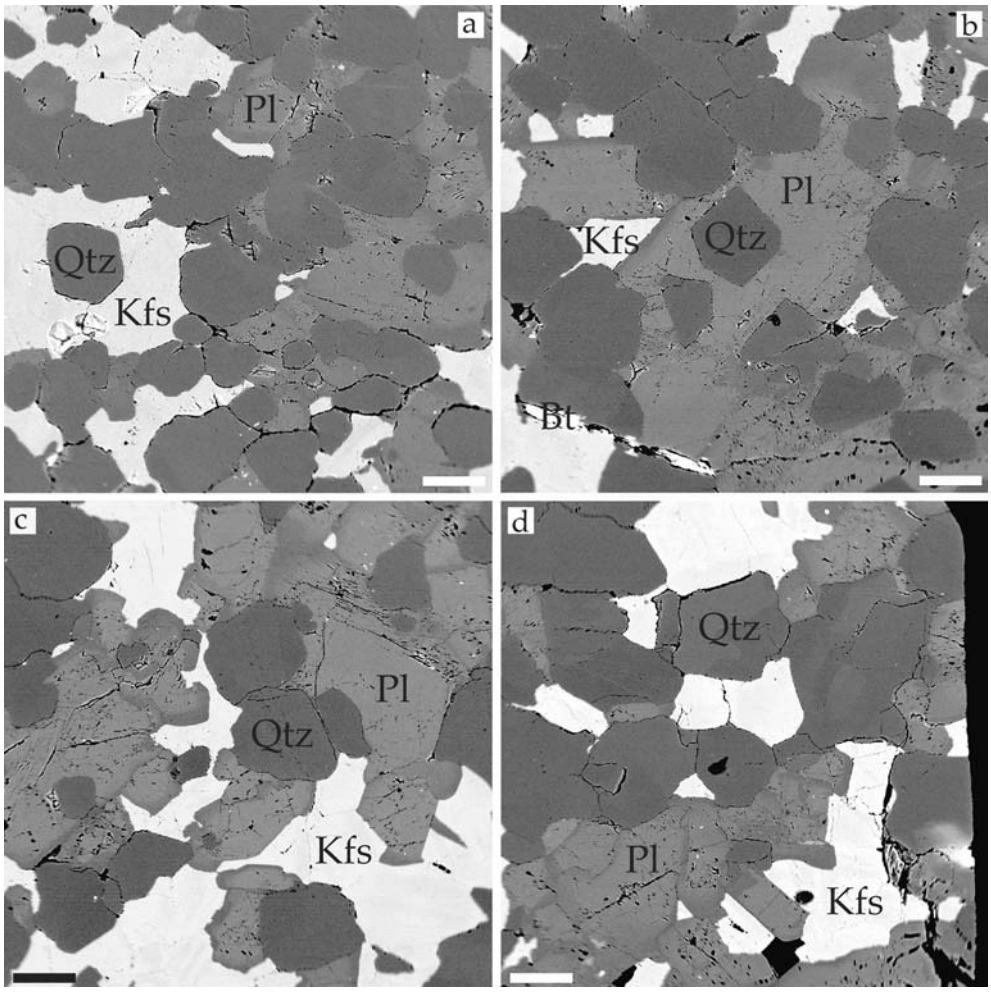

Fig. 1 Backscattered electron images of unreacted aplite cylinders. **a**–**d** represent a longitudinal traverse from the middle to one end of a cylinder ≈7 mm in length. The scale bar is 200 μm long. Mineral symbols after Kretz (1983)

Table 2 Starting materials, conditions, and durations of the conducted experiments

Run no.	Starting materials	Temperature (°C)	H_2O[a] (wt%)	Duration (h)	Phases	Percentage of glass (vol)	Melt thickness (μm)
LT3C-0	H_2O + leucogranite core	25	12.30	144	Qtz + Pl + Kfs + Bt	0	
LT3C-10	H_2O + leucogranite powder	800–850	10.37	96–24	Glass + 1–3%Qtz	97–99	
LT3C-20	H_2O + leucogranite powder	800–850	10.44	96–24	Glass + 1–3% Qtz	97–99	
LT3C-21	H_2O + leucogranite powder	800–850	10.33	96–24	Glass + < 1% Qtz	> 99	
LT3C-19	H_2O + leucogranite core	690	10.24	18	Qtz + Pl + Kfs + Bt + glass	3–4	3–3
LT3C-18	H_2O + leucogranite core	690	10.65	176	Qtz + Pl + Kfs + Bt + glass	4–5	8–14
LT3C-17	H_2O + leucogranite core	690	10.36	365	Qtz + Pl + Kfs + Bt + glass	7–8	12–25
LT3C-16	H_2O + leucogranite core	690	10.23	744	Qtz + Pl + Kfs + Bt + glass	12	25–35
LT3C-23	H_2O + leucogranite core	690	10.47	2,925	Qtz + Pl + Kfs + Bt + glass	20	30–40
LT3C-26	H_2O + leucogranite core	740	0.36	192	Qtz + Pl + Kfs + Bt + glass	8	10–15
LT3C-25	H_2O + leucogranite core	740	1.19	742	Qtz + Pl + Kfs + Bt + glass	14	35–45
LT3C-27	H_2O + leucogranite core	740	1.19	1,464	Qtz + Pl + Kfs + Bt + glass	20	40–60
LT3C-28	H_2O + leucogranite core	740	1.11	2,228	Qtz + Pl + Kfs + Bt + glass	23	50–65
LT3C-13	H_2O + leucogranite core	800	10.44	11	Qtz + Pl + Kfs + glass	12	25–45
LT3C-12	H_2O + leucogranite core	800	9.64	24	Qtz + Pl + Kfs + glass	18	30–55
LT3C-11	H_2O + leucogranite core	800	10.27	123	Qtz + Pl + Kfs + glass	28	55–75
LT3C-14	H_2O + leucogranite core	800	10.23	407	Qtz + Pl + glass	52	145
L3-6	H_2O + leucogranite core	800	9.95	795	Qtz + Pl + glass	66	235
LT3C-15	H_2O + leucogranite core	800	10.54	1,461	Qtz + Pl + glass	77	370

All experiments conducted at 200 Mpa. Mineral symbols after Kretz (1983)
[a]Proportion of water sealed inside the capsule with respect to the granite core

Results

690 and 740°C experiments

Relict grains of all the starting mineral phases together with glass (melt phase at run conditions) are present in the experiments conducted at 690 and 740°C (run durations from 18 to 2,925 h, Table 2, Fig. 2). The glass forms an interconnected network along most of the mineral boundaries and fractures within feldspars, with the main volume of glass occurring as inter-granular films along quartz–feldspars boundaries and at quartz–plagioclase–K-feldspar triple junctions (Fig. 2). The apparent thickness of glass films is roughly constant from edge to core of the rock cylinders, and is equal or slightly greater in triple

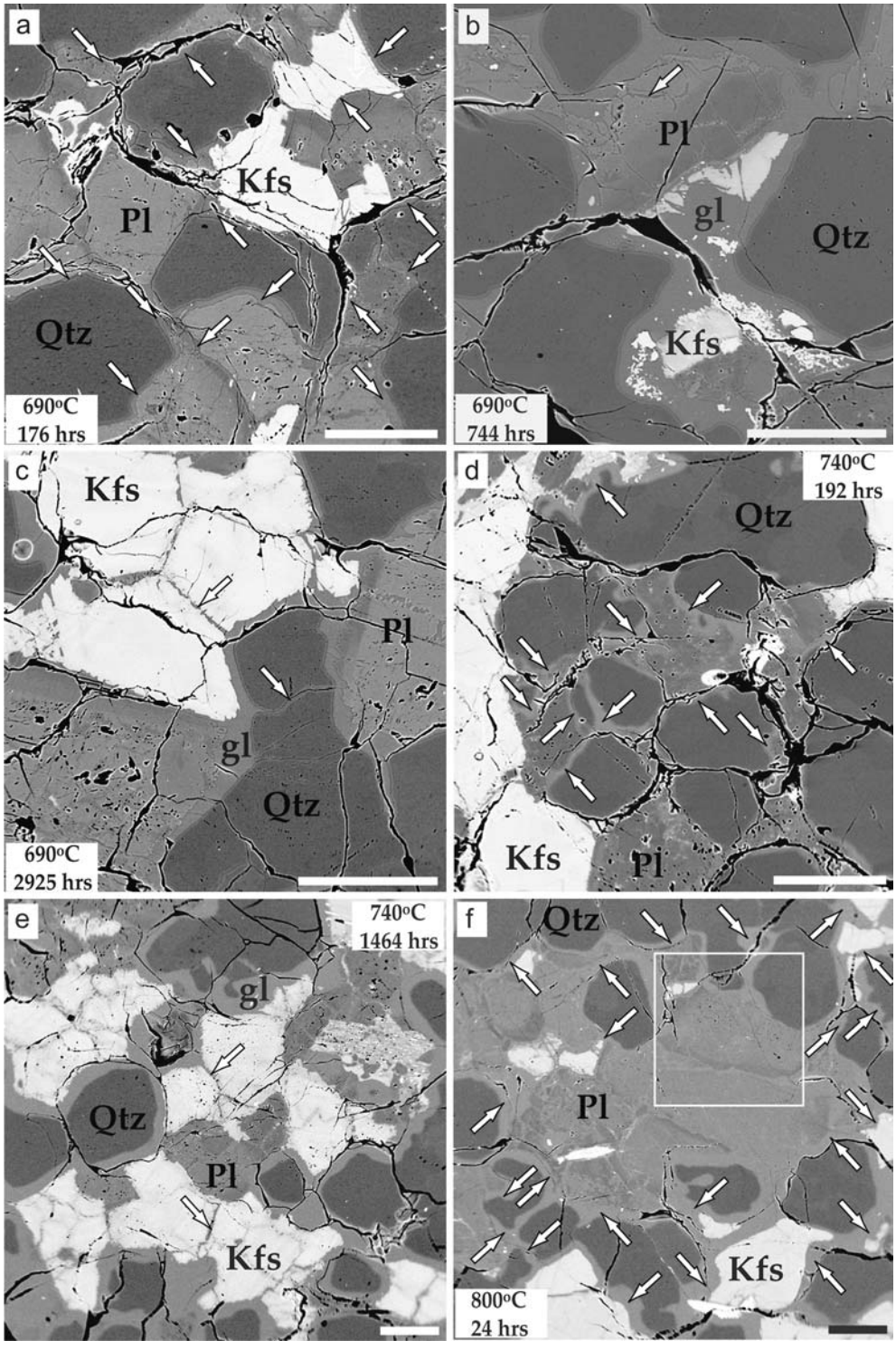

Fig. 2 Backscattered electron images of run products. The scale bar is 200 μm long. *Arrows* in **a**, **d**, **f** point out the presence of glass (former melt) along most mineral interfaces. *Arrows* in **c**, **e** point out the presence of melt in fractures within quartz and K-feldspar. *Arrows* in **g** indicate domains of new feldspars. See text for more explanation. Mineral symbols after Kretz (1983). *gl* glass

Fig. 2 (Contd.)

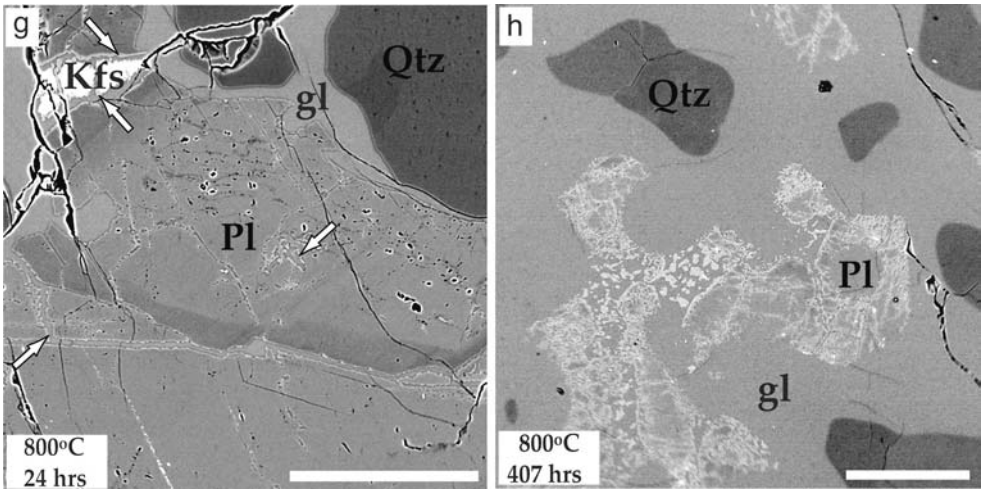

junctions compared with quartz–feldspar boundaries (Table 2). The mean apparent glass thickness and modal percentage of glass increase approximately linearly with the square root of time (Fig. 3). This indicates that the interface reaction and/or diffusion in melt are the rate-limiting processes during melting (Cooper and Kingery 1964; Crank 1975; Zhang et al. 1989; Shaw 2004). Calculated rates of melting of quartz–feldspar boundaries at 690°C are $\approx 8.0\times10^{-12}$ m/s (early stages of melting) and 6.0×10^{-13} m/s (late stages of melting), and $\approx 1.5\times 10^{-11}$ m/s (early stages) and 6.0×10^{-12} m/s (late stages) at 740°C.

For all the 690°C experiments, enough water was added (≈10 wt% H_2O) to saturate the liquid if the charge melted completely. The mean H_2O concentrations in glasses from 690°C experiments (≈7 wt%, Table 3) are comparable to those in H_2O-saturated granite liquids at the same *P–T* conditions (Holtz et al. 1992a). Less water was added in the 740°C runs (≈0.5–1 wt% H_2O) with the intent of producing H_2O-undersaturated melts during progressive melting. Mean H_2O concentrations in glasses from 740°C experiments (≈6.6–5.2 wt%), however, are comparable or slightly less than the saturation value (see Holtz et al. 1992a), and decrease with experimental time (Table 3). In all the experiments at 740°C, added water was consumed by the melting reaction as capsules did not loose any weight after they were punctured and placed in a desiccator. The slow melting rates, however, prevented from achieving liquid compositions well below H_2O saturation (minimum H_2O concentrations in melt at the experimental conditions are ≈4–5 wt%, e.g. Holtz et al. 2001). Glasses from all 690 and 740°C experiments have homogeneous and similar major element compositions within analytical uncertainties (Table 3). They plot on the Qtz–Ab–Or projection of the 200 MPa H_2O cotectic line of the granite system (taken from Winkler 1974), and ≈2.5–5 wt% off the 200 MPa H_2O haplogranite eutectic (Tuttle and Bowen 1958) toward the Qtz–Or sideline (Fig. 4) (hereafter mineral symbols after Kretz 1983). We note, however, that normative anorthite concentrations are higher than those predicted by the granite cotectic line.

800°C Experiments

Quartz, plagioclase and glass are present in all the experiments conducted at 800°C (Table 2, Fig. 2). Biotite decomposes to Ti-Mag + Pl + Crn in less than 24 h of run time. Potassium feldspar is completely consumed between 123 and 407 h. Plagioclase and more rarely K-feldspar partially recrystallize inward to a ternary sodic feldspar solid solution that is both more calcic and potassic than the starting plagioclase (Figs. 2, 5, 6). Recrystallization starts sooner than 24 h, with the new feldspar forming very thin (< 5 μm thick) subhedral and discontinuous films on the rims of starting plagioclase and alkali feldspar crystals (Fig. 2g). After 123 h, the new feldspar constitutes a mostly continuous, ≈1–5 μm thick jacket around relict plagioclase, with sharp and anhedral boundaries between both generations of feldspars (Fig. 5a). Note in Fig. 5a that the dark domains within some of the relict plagioclase adjacent to new feldspar represent compositional zoning in the starting plagioclase (compare with Fig. 1). After 407 h the largest relict plagioclase grains are surrounded by a semi-continuous, euhedral and solid new feldspar rim, ≈5–10 μm thick. This rim is separated from the partially resorbed relict grain by a 5–20 μm thick sieve-textured plagioclase domain that represents a mixture of relict and new minerals (Fig. 5b). The sieve-textured plagioclase is present also locally toward the interior of relict grains, where melt has percolated along fractures. The smaller relict grains are now composed of newly formed solid rims and sieve-textured to skeletal cores, with only small isolated relict feldspar domains remaining in the cores (Fig. 5b, left side). New euhedral feldspars, ≈5–40 μm across, have crystallized in the melt adjacent to relict plagioclases. After 1,461 h, relict plagioclase constitutes only < 5 to 20 μm isolated domains within the cores of new skeletal feldspars (Fig. 5d). The new

feldspar reacts continuously with the liquid and, with increasing run duration, its albite component decreases whereas the anorthite component increases (Fig. 6).

In experiments up to 123 h duration, glass constitutes an interconnected network along most of the mineral boundaries and fractures (Fig. 2) and the mean thickness of inter-granular glass films and modal percentage of glass increase proportionally with the square root of time (Fig. 3), indicating that the rate of melting is controlled by the kinetics of the interface reaction and/or the rate of diffusion in melt (Cooper and Kingery 1964; Crank 1975; Zhang et al. 1989; Shaw 2004). In experiments of 407 h or longer, glass forms a matrix that includes isolated quartz and plagioclase grains (Fig. 2).

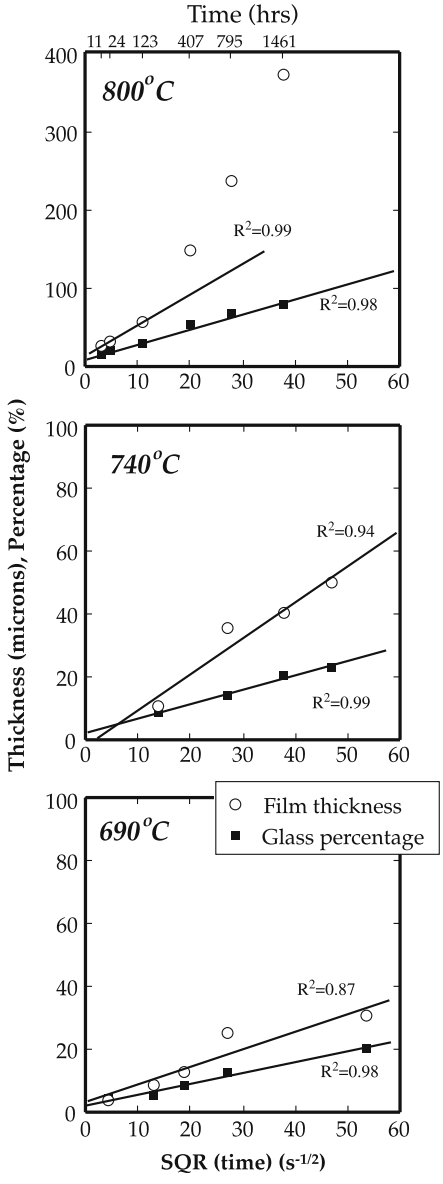

Fig. 3 Mean values of volume percentage of glass and glass film thickness versus experimental temperature and square root of run duration

Calculated rates of melting of quartz–feldspar boundaries are $\approx 8.0\times10^{-11}$ m/s (early stages) and 5.5×10^{-11} m/s (late stages).

Water concentrations in the 800°C experimental glasses (≈5.8–7.3 wt%, Table 4) are comparable to those of H_2O-saturated granite melts at the same *P–T* conditions (Holtz et al. 1992a). Glass compositions in the 800°C experiments are heterogeneous. At any given experimental duration they form linear arrays in (pseudo-ternary) wt% normative Qtz–Ab–Or space, with approximately constant normative albite/anorthite/orthoclase ratios and highly variable quartz/feldspar ratios (Fig. 4). In the short duration experiments glass compositions are displaced toward the orthoclase corner with respect to the 200 MPa H_2O haplogranite eutectic. With increasing run duration they migrate toward the bulk composition of the sample, such that melts next attain the albite/anorthite/orthoclase proportion of the starting bulk composition (between 407 and 795 h), and then finally approach the bulk quartz/feldspar ratio much more slowly.

At each experimental duration Al_2O_3, CaO, Na_2O, and K_2O concentrations in glass decrease with increasing silica, whereas FeO_t and H_2O are constant within analytical uncertainties through the entire charge (Fig. 7). For any given experiment, the ASI and Al/Na molar ratios in glass are constant through the entire charge, whereas Al/Ca increases and Al/K decreases toward SiO_2-rich domains. Compositional gradients in melt are present in all experiments in which glass films are thick enough to permit conducting analytical transverses (experiments with a duration ≥407 h) (Fig. 8). Figure 9 shows glass composition as a function of the adjacent mineral phase, taking the 123-h experiment as example. Some oxide components reflect the neighboring mineral phase. For instance, Al_2O_3 is greater close to feldspars whereas SiO_2 is higher close to quartz. Concentrations of Na_2O, K_2O and CaO, however, do not correspond to the composition of the adjacent feldspar, and all are slightly elevated near plagioclase and K-feldspar. Although molar Al/Na is constant throughout the entire melt, Al/Ca is greater adjacent to quartz than feldspar, whereas Al/K is greater adjacent to feldspar than quartz. As a result, the ASI is roughly constant in melts close to feldspars, quartz, or in triple junctions.

Discussion

Distribution of melt

Backscattered electron imaging of run products shows that the melt (now glass) forms an interconnected network throughout most of the mineral boundaries and fractures in two dimensional sections of runs at any experimental temperature and duration, and is not preferentially located at Qtz–Pl–Kfs triple junctions or segregated in discrete pools (Fig. 2). The main volumes of glass are approximately equally distributed in Qtz–Pl–Kfs

Table 3 Mean compositions (wt%) of glasses in the 690 and 740°C core melting experiments

Run *T*, duration No. analyses	LT3C-18 690°C, 176 h 5	LT3C-17 690°C, 365 h 10	LT3C-16 690°C, 744 h 38	LT3C-23 690°C, 2,925 h 42	LT3C-26 740°C, 192 h 3	LT3C-25 740°C, 742 h 49	LT3C-27 740°C, 1,464 h 48	LT3C-28 740°C, 2,228 h 65
SiO_2	69.87 (0.43)	71.64 (0.68)	71.58 (0.64)	73.31 (0.51)	70.71 (1.93)	73.20 (0.55)	73.50 (0.74)	74.04 (0.54)
Al_2O_3	13.45 (0.11)	12.20 (0.13)	12.07 (0.26)	11.79 (0.16)	13.24 (1.40)	12.03 (0.20)	12.05 (0.16)	11.87 (0.20)
FeO[a]	0.59 (0.17)	0.35 (0.09)	0.28 (0.06)	0.26 (0.06)	0.45 (0.14)	0.31 (0.04)	0.28 (0.04)	0.32 (0.06)
MnO	0.04 (0.02)	0.03 (0.01)	0.02 (0.01)	0.02 (0.01)	0.01 (0.00)	0.01 (0.01)	0.01 (0.01)	0.01 (0.01)
MgO	0.12 (0.01)	0.07 (0.01)	0.08 (0.02)	0.05 (0.01)	0.10 (0.07)	0.04 (0.01)	0.05 (0.01)	0.06 (0.01)
CaO	0.30 (0.04)	0.35 (0.06)	0.39 (0.04)	0.33 (0.03)	0.19 (0.03)	0.27 (0.03)	0.25 (0.03)	0.26 (0.03)
BaO	0.00 (0.01)	0.01 (0.01)	0.01 (0.01)	0.01 (0.01)	0.00 (0.00)	0.01 (0.01)	0.01 (0.01)	0.01 (0.01)
Na_2O	3.70 (0.19)	3.52 (0.17)	3.43 (0.11)	3.71 (0.09)	3.71 (0.34)	3.52 (0.13)	3.65 (0.11)	3.58 (0.11)
K_2O	4.17 (0.12)	4.07 (0.13)	4.23 (0.12)	4.13 (0.13)	4.88 (0.12)	4.65 (0.12)	4.54 (0.12)	4.62 (0.11)
F	0.08 (0.06)	0.04 (0.04)	0.14 (0.07)	0.02 (0.03)	0.20 (0.23)	0.11 (0.09)	0.05 (0.05)	0.10 (0.08)
F = O	−0.03	−0.02	−0.06	−0.01	−0.08	−0.05	−0.02	−0.04
H_2O by diff	7.71 (0.41)	7.72 (0.81)	7.83 (0.61)	6.38 (0.54)	6.59 (0.69)	5.90 (0.58)	5.60 (0.76)	5.17 (0.59)
#Mg	0.27 (0.03)	0.27 (0.03)	0.33 (0.05)	0.26 (0.04)	0.27 (0.08)	0.19 (0.03)	0.22 (0.03)	0.25 (0.04)
ASI	1.208 (0.028)	1.128 (0.041)	1.105 (0.028)	1.056 (0.026)	1.127 (0.058)	1.064 (0.031)	1.060 (0.026)	1.045 (0.025)
Moles Al/Na	2.22 (0.11)	2.11 (0.11)	2.14 (0.08)	1.93 (0.06)	2.17 (0.04)	2.08 (0.08)	2.01 (0.06)	2.02 (0.07)
Moles Al/K	2.98 (0.10)	2.77 (0.10)	2.64 (0.08)	2.64 (0.09)	2.50 (0.20)	2.39 (0.08)	2.45 (0.07)	2.37 (0.06)
Norm Qtz	31.04	34.42	34.23	34.91	29.51	34.02	34.04	34.61
Norm Ab	31.31	29.79	29.02	31.39	31.39	29.79	30.89	30.29
Norm Or	24.64	24.05	25.00	24.41	28.84	27.48	26.83	27.30
Norm An	1.49	1.74	1.93	1.64	0.94	1.34	1.24	1.29
Norm Hy	1.46	0.87	0.75	0.64	1.09	0.69	0.66	0.76
Norm Crn	2.30	1.37	1.14	0.62	1.51	0.72	0.68	0.51
Norm Ab/An	21.01	17.12	15.04	19.14	33.39	22.23	24.91	23.48

[a]Total Fe as FeO

triple junctions and along quartz–plagioclase and quartz–K-feldspars boundaries. Glass is less abundant along plagioclase–K-feldspar boundaries and in fractures within feldspars. Although present, glass is rare in between quartz grains and in fractures within quartz (Fig. 2c). Melt interconnection likely occurs also in three dimensions. This is supported by homogeneous melt compositions in 690 and 740°C experiments, and by homogeneous melt Al/Na and ASI ratios throughout the individual 800°C experiments. These observations indicate that H_2O-saturated melting in quartzo-feldspathic protoliths under hydrostatic pressure conditions will form an interconnected network of granitic melt throughout the protolith even at very low degrees of partial melting (e.g. ≤ 5 vol% in the 690°C experiments, Table 2). The current results are in accordance with: (1) previous studies on the static, H_2O-saturated and H_2O-undersaturated partial melting of granite, schist, gneiss, granulite and diatexite cores (Mehnert et al. 1973; Büsch et al. 1974; Arzi 1978; Brearley and Rubie 1990); (2) the low median dihedral angles of crystal–crystal-melt junctions measured in static equilibrium melt texture experiments, which suggest that melt interconnection in a crustal protolith should be established at very low melt fractions, even with low a_{H2O} in melt (Jurewicz and Watson 1985; Laporte 1994; Laporte and Watson 1995; Laporte et al. 1997; Lupulescu and Watson 1999; Laporte and Provost 2000); and (3) melt distributions found within statically partially melted crustal rocks in nature in contact aureoles (e.g. Rosenberg and Riller 2000; Holness et al. 2005).

The 740°C and particularly the 690°C experiments were expected to produce melt only at quartz–plagioclase–K-feldspar triple junctions in contact with H_2O fluid, because temperatures were slightly above the water-saturated haplogranite and granite solidi, and below the H_2O-saturated quartz–albite and quartz–orthoclase eutectics (Tuttle and Bowen 1958; Shaw 1963; Luth 1969; Winkler 1974; Johannes 1984, 1989). However, melt is common in quartz–plagioclase and quartz–K-feldspars boundaries. Mehnert et al. (1973) provided several explanations for the same observation in their core melting experiments: (1) the percolation of H_2O through the rock cylinder along grain boundaries, fractures and cleavage cracks; (2) the presence of fine-grain or submicroscopic aggregates of the missing eutectic phase; (3) the presence of the missing eutectic phase as a chemical component in the ternary feldspar solid solution; and/or (4) the migration of melt along grain boundaries and cracks governed by adhesion effects relative to the respective minerals. Back-scattered electron images from the current experiments indicate that the melt network is not created by advancing inward from the edges of the sample or outward from triple junctions, but is likely established instantaneously throughout the entire rock volume. The presence of melt along most of the mineral boundaries can be explained by the early infiltration of water through fractures and mineral boundaries in the rock core, including the initial room-temperature pressurizing step. Hence, melting along grain boundaries between only two phases (quartz–plagioclase, quartz–K-feldspar) may have been

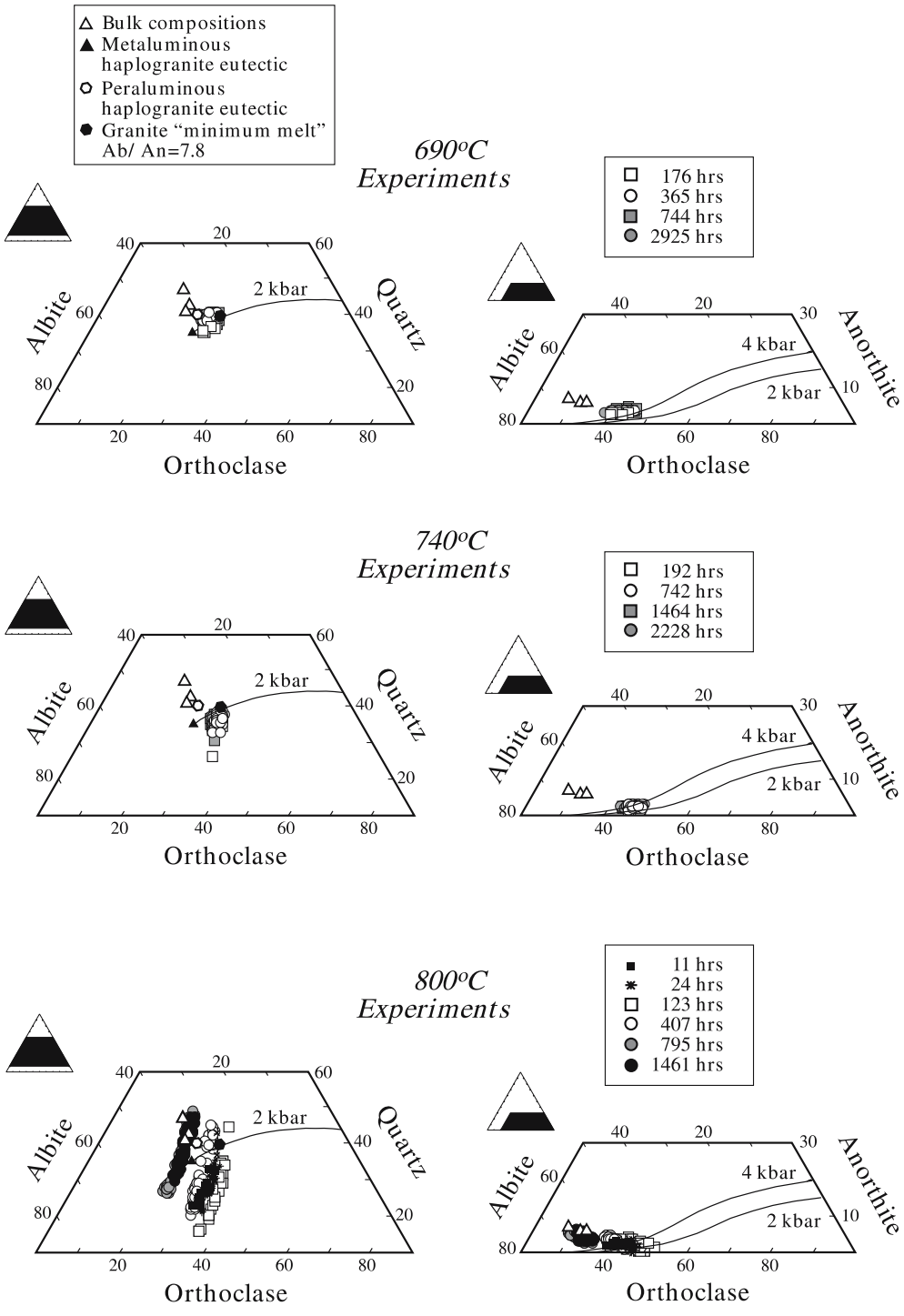

Fig. 4 Weight percentage normative Qtz–Ab–An–Or composition of experimental glasses as a function of experimental temperature and run duration. The normative composition of the starting bulk composition, the 2 kbar H_2O metaluminous and peraluminous haplogranite eutectic (from Tuttle and Bowen 1958; Holtz et al. 1992b), and 2 and 4 kbar H_2O granite cotectic lines (from Winkler 1974) are also shown. Compositions in Qtz–Or–Ab diagrams are projected from An and H_2O. Compositions in Ab–An–Or diagrams are projected from Qtz and H_2O

aided by the transport of necessary components (i.e. those components of the eutectic missing from the assemblage) through aqueous fluid.

Composition of melt

To accurately discuss kinetic data in petrology it is critical to choose the most appropriate phase equilibrium diagrams available for the system under investigation. Approximately 99 wt% of the aplite cylinders are haplogranitic (Table 1); excess Al_2O_3 and extra components FeO and CaO, however, might cause a deviation of the location of eutectic/minimum and cotectic lines with respect to those in the haplogranite system (Tables 1, 3, 4). The system under investigation is metaluminous to slightly peraluminous (ASI≈1.02–1.05); the small variation produced by excess Al_2O_3 on

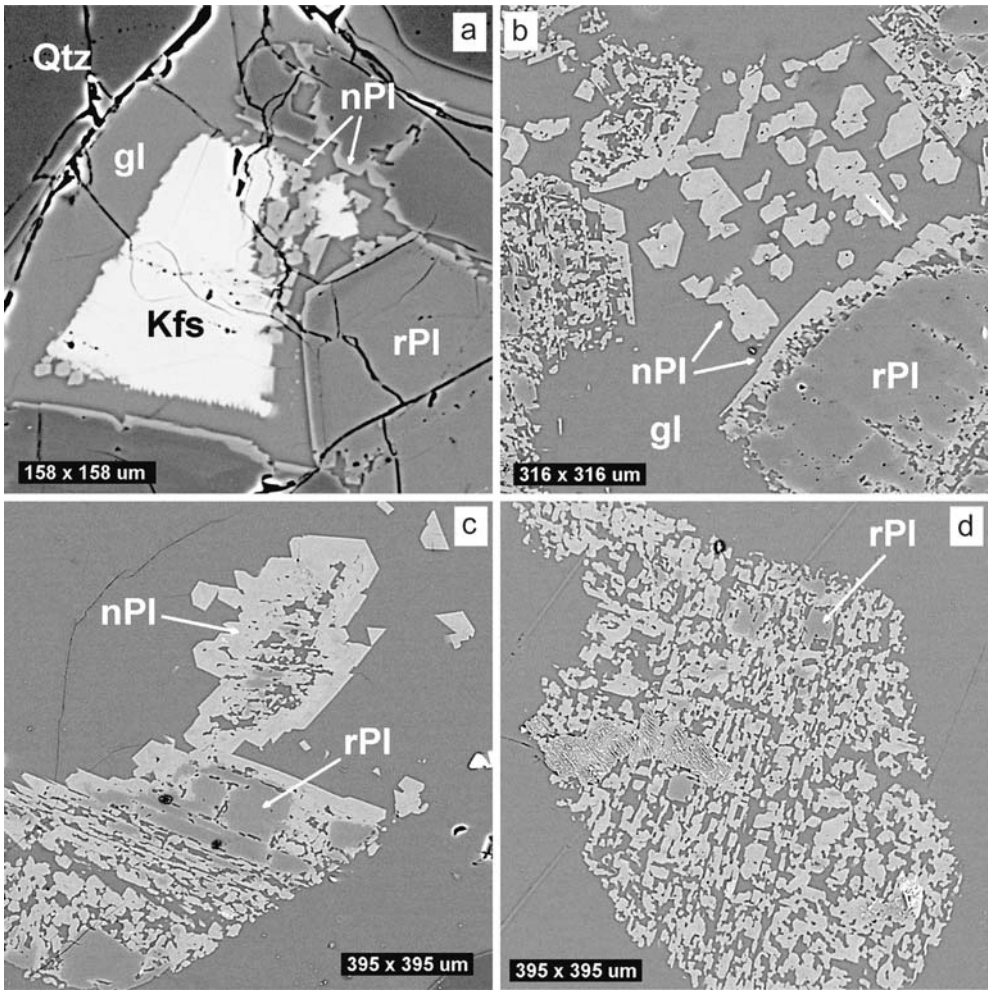

Fig. 5 Backscattered electron images of feldspars in the 800°C experiments. See text for explanation. Mineral symbols after Kretz (1983). *rPl* relict plagioclase, *nPl* new plagioclase, *gl* glass

haplogranite phase equilibria (Holtz et al. 1992b) indicates that its effect in the current system is probably null. There are not experimental studies on the effect of ferromagnesian components on the composition of the minimum in the granite system. The small decrease in the wet solidus temperature when ferromagnesian phases are added to the granite system (e.g. Johannes 1985), together with the very low concentrations of FeO in the current experimental melts (0.10–0.60 wt%), suggest that FeO has a very minor effect on phase equilibria in the current experiments. In spite of several experimental studies, the composition of coexisting feldspars and liquids in equilibrium along the cotectic line of the granite system is not well known (see Winkler 1974; Johannes 1984; Johannes and Holtz 1992). This is due to the sluggish kinetics of equilibration between melt and plagioclase (Johannes 1978, 1980; Johannes and Holtz 1992). We compare our results with the minimum melt compositions and cotectic line of the H_2O-saturated Qtz–Ab–Or–An system at 2 kbar (see Winkler 1974) (Fig. 4). Note, however, that Johannes (1978, 1980, 1984) considers that equilibrium between coexisting granite liquid and feldspars was probably not reached in experiments by Winkler and coworkers. It is also convenient to use as a reference the phase diagrams for the H_2O-saturated haplogranite system (Tuttle and Bowen 1958) (Fig. 10), due to the well-known location of the liquidus surfaces in this system and the low anorthite component of the aplite cylinders.

The composition of melts in the 690°C experiments are reasonably similar to that predicted by current equilibrium phase diagrams (Tuttle and Bowen 1958; Winkler 1974) (Figs. 4, 10); the small deviation with respect to the 2 kbar H_2O haplogranite eutectic can be related to the small anorthite component of the current experimental system. Hence the data indicates that partial melting at the H_2O-saturated granite solidus produces homogeneous, near-minimum temperature melts. Note, however, that the system is not in equilibrium. Anorthite contents of melts are higher than predicted (Fig. 4), which would be expected if plagioclase melts stoichiometrically. Backscattered electron images indicate that feldspars do not show any noticeable change in texture in all the 690°C runs, strongly suggesting that equilibrium, if achieved, is restricted to feldspar-melt interfaces (compare BSE images of feldspars in the 690 vs. 800°C experiments, Figs. 2, 5). The compositions of experimental glasses and starting plagioclase indicate a slight fractionation of plagioclase components (Ab/An

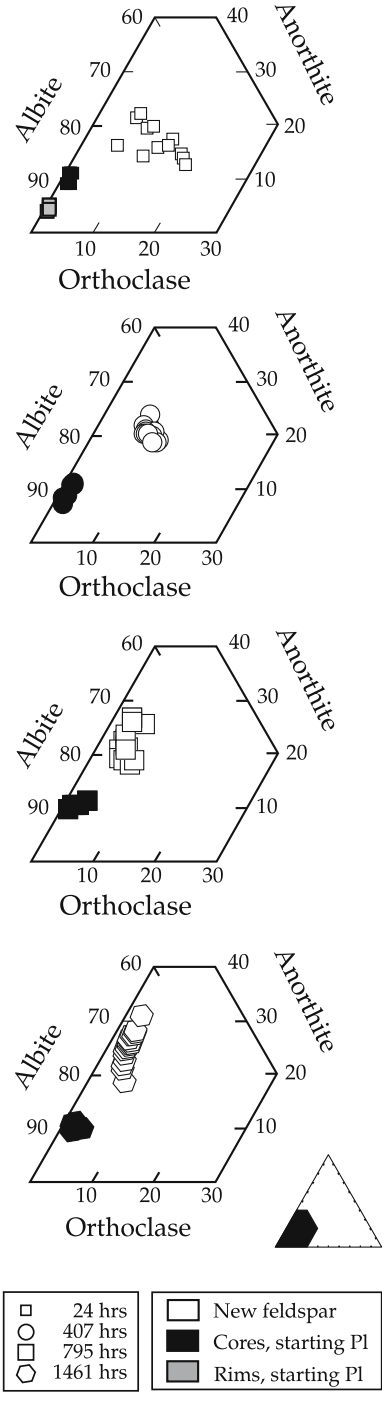

Fig. 6 Weight percentage normative Ab–An–Or composition of starting and experimental feldspars in the 800°C runs as a function of experimental duration

ratio) upon melting (Tables 1, 3). This can be explained either by a tendency of interface melts and feldspars to equilibrate and/or by the supply of albite component to the melt through the dissolution of K-feldspar.

Melting at 740°C produced, as in the 690°C experiments, homogeneous liquids of near-minimum melt composition at the appropriate P–X conditions (Figs. 4, 10). However, melts do not have equilibrium compositions (Fig. 10). First, the compositions of starting plagioclase and experimental glasses (Tables 1, 3) together with BSE imaging (Fig. 2) suggest that melt and feldspars equilibrate only at the interfaces. Second, following Winkler (1974) melts in the granite system leave the cotectic line 15–20°C after the beginning of melting; the melting temperature of 740°C is about 50–70°C above the minimum temperature (Tuttle and Bowen 1958; Winkler 1974; Johannes 1984) and, therefore, 740°C liquids should be displaced toward the quartz–albite sideline with respect to the cotectic, according to the starting bulk composition (see also Fig. 10). Also, following Johannes (1984) the temperature of 740°C is the highest temperature for melts coexisting with quartz, alkali feldspar and plagioclase at $P_{H2O} = 2$ kbar, and plagioclase coexisting with those melts should be close to An_{100}. We notice that although the modal percentage of melt clearly increases with run time (Table 1), liquids in the 740°C runs show almost no change in composition as a function of textural location (triple junctions versus quartz–plagioclase or quartz–K-feldspars boundaries) or experimental duration (from 192 up to 2,228 h) (Table 3, Figs. 4, 10). These observations require that: (1) quartz and feldspars dissolve at a constant proportion such that the resulting bulk liquid is of minimum melt composition; and (2) diffusion through melt is rapid in order to homogenize the mm-sized melt network in the timeframe of the experiments. As diffusivities in melt at 740°C seem to be rapid enough, we can only surmise that the failure of liquids to evolve toward the equilibrium composition must result from sluggish interface reaction kinetics at this temperature. Note also that homogeneous melts in disequilibrium with coexisting mineral phases are characteristics known as typical of solely interface reaction-controlled mineral dissolution processes (e.g. Donalson 1985).

Overall, the above data and discussion indicate that at the current experimental conditions (H_2O-saturated melting of granitic protoliths with an infinite rate of heating), the rate of melting at temperatures around or slightly above (≈50–70°C) the granite solidus is controlled by the kinetics of the interface reaction (and not by diffusion in melt). When that happens, homogeneous disequilibrium melts of near-minimum composition form and persist metastably for some time.

At 800°C melt composition is heterogeneous at any experimental duration (Fig. 7) and compositional gradients throughout the melt are always present (Fig. 8). Interface liquids tend to equilibrate with neighboring mineral phases whereas melts away from interfaces are located in between (Figs. 8, 9, 10); thus melt compositions are controlled by local equilibrium and the diffusive transport properties of melt. We are uncertain, however, if interface liquids are in equilibrium with mineral phases: the anorthite component may change the location of liquidus surfaces in the granite system with respect to those in the haplogranite system. Hence

Table 4 Mean compositions (wt%) of glasses in the 800°C core melting experiments

Run	LT3C-13	LT3C-12	LT3C-11	LT3C-14	L3-6	LT3C-15
Duration	11 h	24 h	123 h	407 h	795 h	1,461 h
No. analyses	15	25	31	59	45	57
SiO_2	69.20 (1.23)	70.80 (1.82)	69.73 (2.53)	71.44 (3.04)	70.81 (2.22)	72.85 (1.83)
Al_2O_3	13.66 (0.66)	13.11 (1.06)	13.09 (1.38)	13.30 (1.73)	13.06 (1.21)	12.00 (1.11)
FeO[a]	0.30 (0.13)	0.32 (0.15)	0.16 (0.06)	0.09 (0.08)	0.22 (0.02)	0.31 (0.04)
MnO	0.01 (0.01)	0.01 (0.01)	0.00 (0.00)	0.01 (0.01)	0.01 (0.01)	0.00 (0.01)
MgO	0.03 (0.02)	0.03 (0.02)	0.02 (0.01)	0.04 (0.02)	0.04 (0.01)	0.04 (0.01)
CaO	0.29 (0.05)	0.30 (0.10)	0.35 (0.13)	0.42 (0.16)	0.58 (0.12)	0.48 (0.14)
BaO	0.02 (0.01)	0.02 (0.02)	0.01 (0.01)	0.02 (0.02)	0.02 (0.02)	0.02 (0.02)
Na_2O	4.35 (0.28)	4.09 (0.36)	4.06 (0.49)	4.32 (0.56)	4.69 (0.43)	4.19 (0.34)
K_2O	4.87 (0.11)	4.94 (0.23)	5.30 (0.22)	4.54 (0.30)	3.30 (0.16)	3.22 (0.16)
F	0.14 (0.09)	0.07 (0.07)	0.05 (0.05)	0.05 (0.06)	0.03 (0.04)	0.10 (0.09)
F = O	−0.06	−0.03	−0.02	−0.02	−0.01	−0.04
H_2O by diff	7.19 (0.93)	6.34 (0.67)	7.23 (0.72)	5.80 (0.58)	7.26 (0.47)	6.84 (0.45)
#Mg	0.13 (0.06)	0.15 (0.05)	0.17 (0.07)	0.46 (0.20)	0.25 (0.06)	0.17 (0.04)
ASI	1.055 (0.031)	1.038 (0.031)	1.002 (0.026)	1.039 (0.026)	1.059 (0.019)	1.066 (0.029)
Moles Al/Na	1.91 (0.08)	1.95 (0.09)	1.97 (0.07)	1.87 (0.06)	1.69 (0.04)	1.74 (0.06)
Moles Al/K	2.59 (0.11)	2.45 (0.12)	2.28 (0.17)	2.70 (0.20)	3.65 (0.19)	3.44 (0.20)
Norm Qtz	24.33	27.14	24.92	27.89	29.41	34.81
Norm Ab	36.81	34.61	34.35	36.55	39.69	35.45
Norm Or	28.78	29.19	31.32	26.83	19.50	19.03
Norm An	1.44	1.49	1.74	2.08	2.88	2.38
Norm Hy	0.64	0.68	0.34	0.28	0.52	0.67
Norm Crn	0.71	0.49	0.04	0.52	0.72	0.75
Norm Ab/An	25.56	23.23	19.74	17.57	13.78	14.89

[a]Total Fe as FeO

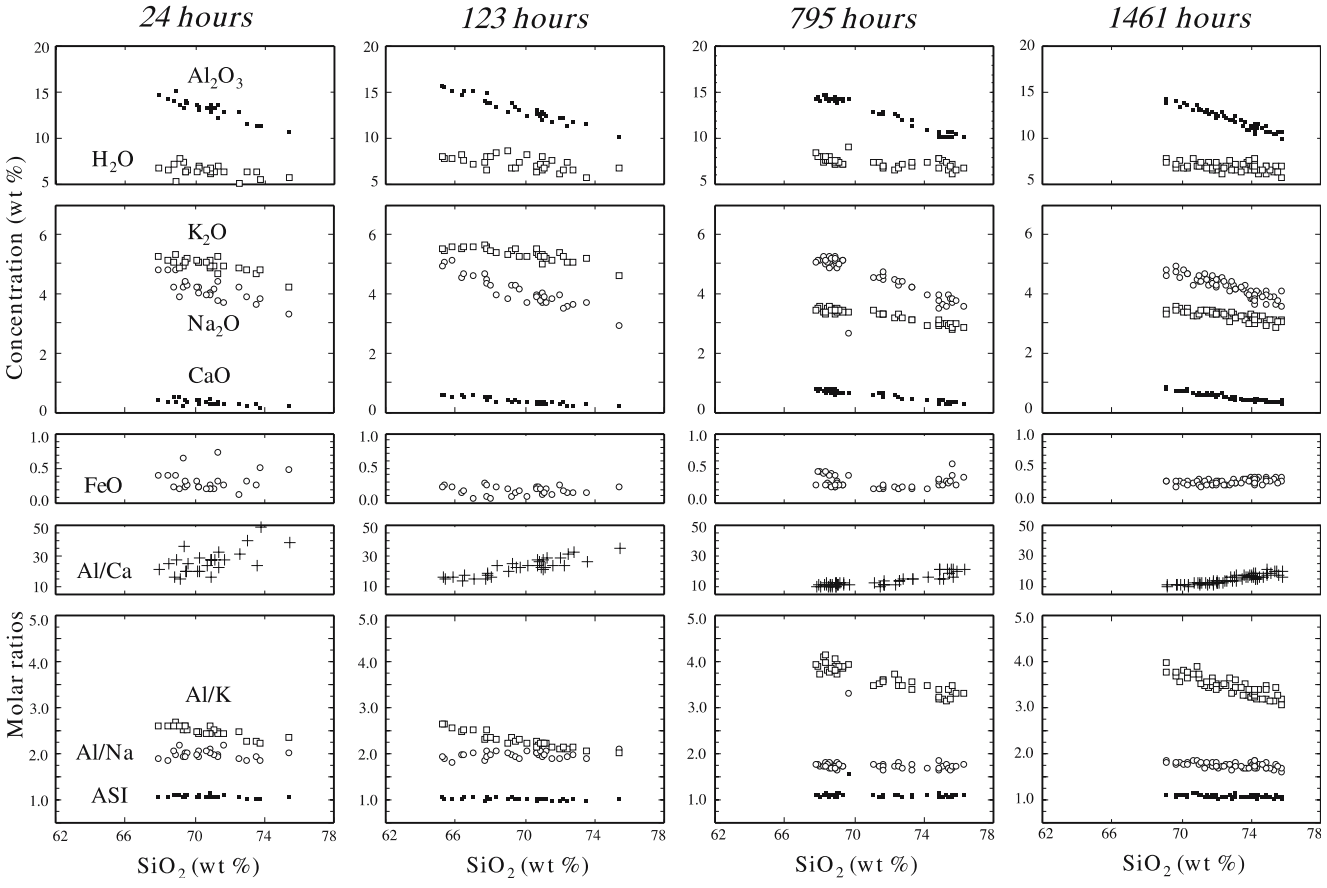

Fig. 7 Composition of the 800°C experimental glasses (analyzed throughout the entire charge and in the several textural locations) as a function of run duration

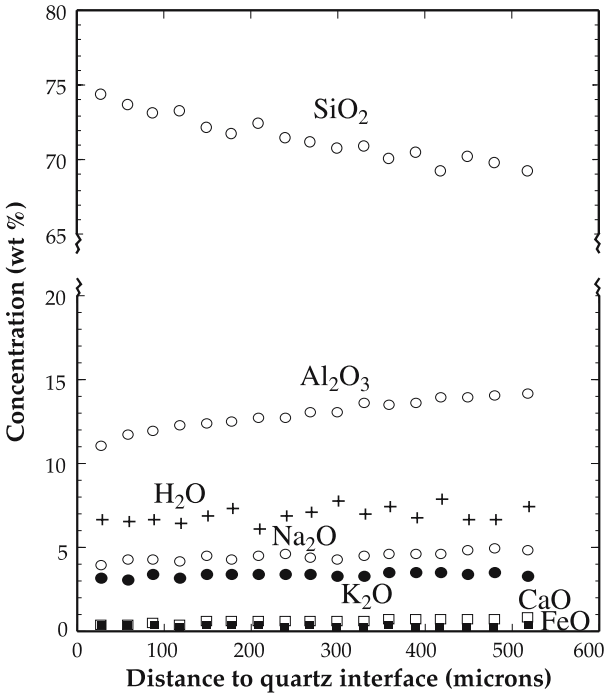

Fig. 8 Compositional transverse in glass of the 1,461-h 800°C experiment located in between quartz (to the *left*) and plagioclase (to the *right*)

we are uncertain if melting is solely controlled by diffusion in melt, or diffusion and interface reaction (Fig. 3). Eventually, all liquids tend to evolve toward the equilibrium composition (Figs. 4, 10). The experimental melts at a given duration are not spread through the entire pseudo-ternary Qtz–Ab–Or space within the appropriate isotherms. Instead, they form linear trends at high angle with the cotectic line, located between the 800°C isotherms for quartz and feldspars, with early liquids located toward the quartz–orthoclase sideline with respect to the eutectic (Fig. 10). These arrays formed by glasses from single experimental duration can be explained by the diffusive transport properties of the melt (e.g. Watson 1982; Baker 1990, 1991; Mungall et al. 1998; Acosta-Vigil et al. 2002, 2006). The spread of the data in the quartz–feldspar direction is due to the low diffusivities of SiO_2 and Al_2O_3: the concentrations of SiO_2 and Al_2O_3 are higher in melts close to quartz or feldspars, respectively (Fig. 9). The nearly constant albite/orthoclase ratio of the linear arrays at any experimental duration is due to: (1) the stoichiometry of the Al–Na–K diffusing component, (2) the much higher diffusivities of the alkalis (compared with Al and Si), and (3) the long range chemical communication in the system via chemical potential gradients, operative throughout the entire melt volume independently of distance (see Acosta-Vigil et al. 2002, 2006). Early liquid compositions are more potassic than the eutectic due to more rapid dissolution of K-feldspar compared to plagioclase. This may stem, at least in part, from the recrystallization of plagioclase to form a more primitive, ternary phase (appropriate to temperature). Once K-feldspar is completely consumed from the system (between 123 and 407 h, Table 2), liquid compositions migrate back toward the bulk rock composition. During the process, the temporary location of any of the liquids on the eutectic does not have any significance regarding temperature of melting or composition of the source rock.

The above data and discussion indicate that at the current experimental conditions, the rate of melting at temperatures well above (≈100–130°C) the solidus is controlled both by diffusion in melt (during melting of quartz) and the kinetics of the interface reaction (during melting of feldspars), though this conclusion might depend on the bulk composition of the system. Also, melting at temperatures well above the solidus produces disequilibrium, heterogeneous liquids whose compositions are largely controlled by the diffusive transport properties of the melt and local equilibrium with neighboring mineral phases. We emphasize that long range (mm-scale in these experiments) chemical communication occurred within the silicate liquid, reflected by homogeneous melt ASI and Al/Na molar ratios throughout the entire reservoir.

Results from previous experimental programs on rock melting involving a variety of systems (granitic, pelitic, basaltic), starting materials (solid cores versus powdered rocks), a_{H2O} (dry to H_2O-saturated), temperatures (660–1,350°C), pressures (0–10 kbar) and run durations (0–3,743 h) (Mehnert et al. 1973; Watson and Jurewicz 1984; Brearley and Rubie 1990; Tsuchiyama 1985a; Hammouda and Pichavant 1999, 2000; Devineau et al. 2005) have also found that melting around the solidus produces homogeneous melts, whereas melting at temperatures well above the solidus produces heterogeneous disequilibrium liquids. Comparable results among this and previous experimental programs suggest that (1) there are systematic behaviors for the kinetics of melting of natural mineral assemblages, and (2) the temperature overstep of the melting reaction has a larger effect on the kinetics behavior of melting than the actual temperature at which melting occurs.

Equilibration between melt and feldspars

Two contrasting, end member mechanisms of equilibration between melt and feldspar solid solutions include: (1) the diffusive transport of components through liquid and solid (e.g. Tsuchiyama and Takahashi 1983; Tsuchiyama 1985a, 1985b); and (2) re-crystallization of residual feldspars to new equilibrium feldspars (likely via dissolution into, and re-precipitation from, the liquid) (e.g. Wark and Stimac 1992; Nakamura and Shimakita 1998; Hammouda and Pichavant 2000; Devineau et al. 2005). During equilibration through diffusive transport, diffusion within feldspars would be the rate-limiting process (e.g. Tsuchiyama and Takahashi 1983; Tsuchiyama 1985a, 1985b), and diffusion profiles are expected to occur within at least the solids. Using

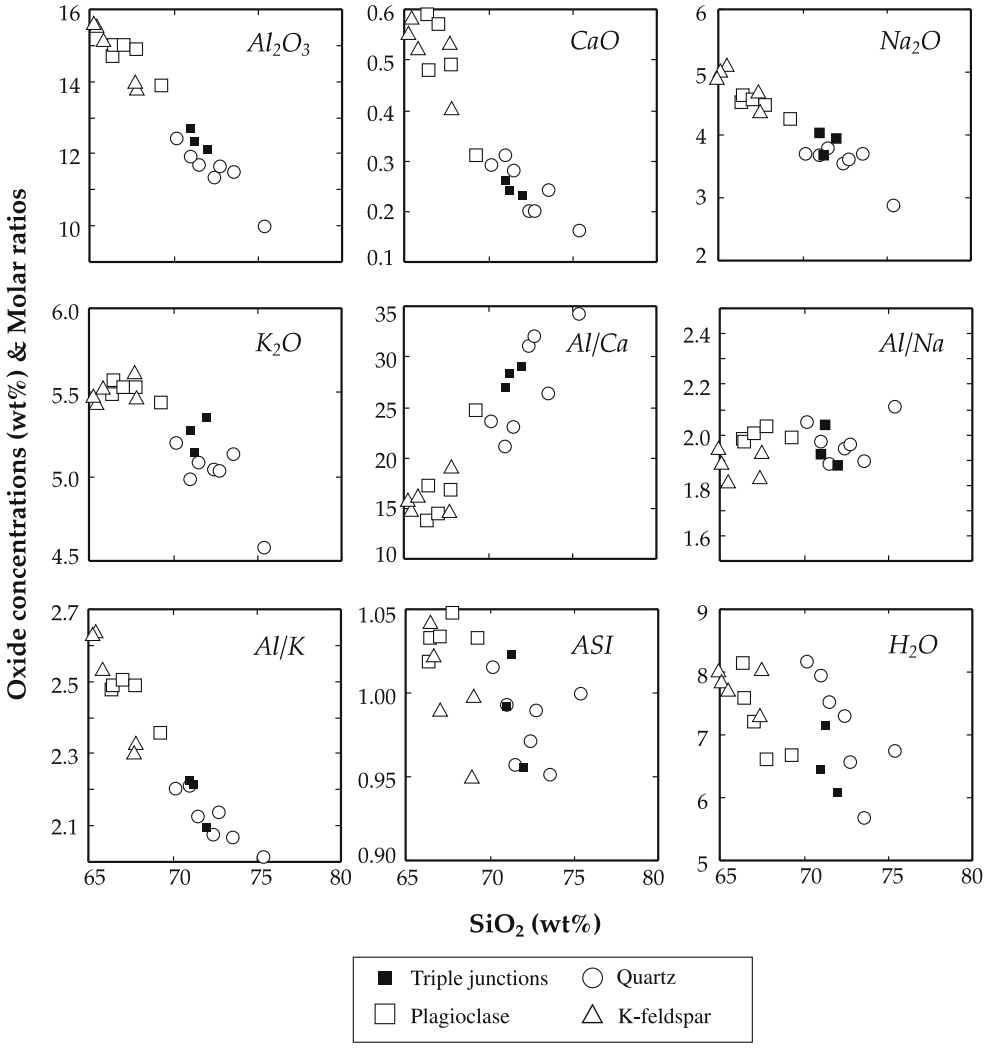

Fig. 9 Composition of the 123-h 800°C experimental glasses (analyzed throughout the entire charge) as a function of textural location

diffusion coefficients from Giletti and Shanahan (1997) and the approximation $x^2 = Dt$, the length scale of expected alkali diffusion profiles within feldspars after 2–3 months at 700 and 800°C is ≈1 and 10 μm, respectively; diffusion processes within feldspars in the current experiments, therefore, would be undetectable. During equilibration by re-crystallization, the slower process between diffusion in melt and interface reaction will likely determine the rate at which equilibrium is approached.

Backscattered electron images and EMP analyses of the 690 and 740°C experimental runs indicate that practically all the feldspar component of the rock does not change either texture or composition (with respect to the starting feldspar) during the experiments, and does not equilibrate with the homogeneous melts produced at these temperatures except perhaps right at the interfaces (compare with Fig. 3 of Johannes 1984). Although the absence of any measurable diffusion profiles within feldspars does not imply that diffusion through liquid and solid has not constituted a major mechanism during feldspar-melt equilibration, the previous discussion strongly suggests that the sluggish interface reaction may have controlled as well the rate of equilibration at or slightly above the wet granite solidus, as concluded by Johannes (1978, 1980, 1989) and Johannes and Holtz (1992).

During the 800°C experiments feldspars change texture and composition rapidly, and the bulk feldspar component of the rock recrystallizes entirely in about 2 months. The results are comparable to previous plagioclase melting experimental studies at high temperatures (875–1,420°C) in which euhedral, newly crystallized plagioclase formed rapidly around partially resorbed starting plagioclase, with a large compositional step between both generations of feldspar; i.e. no diffusion gradients seem to be present across the boundary (Johannes 1989; Johannes and Holtz 1992; Wark and Stimac 1992; Nakamura and Shimakita 1998; Hammouda and Pichavant 2000). Equilibration between feldspars and interface melts at temperatures well above the wet solidus (800°C experiments) and at H_2O-saturation

involves dissolution of relict feldspar and crystallization of euhedral, new equilibrium phase (Fig. 5). The rate of equilibration at these conditions, however, still might be controlled by the kinetics of the interface reaction, as in the current experiments interface melts seem to be always undersaturated in plagioclase (Fig. 10).

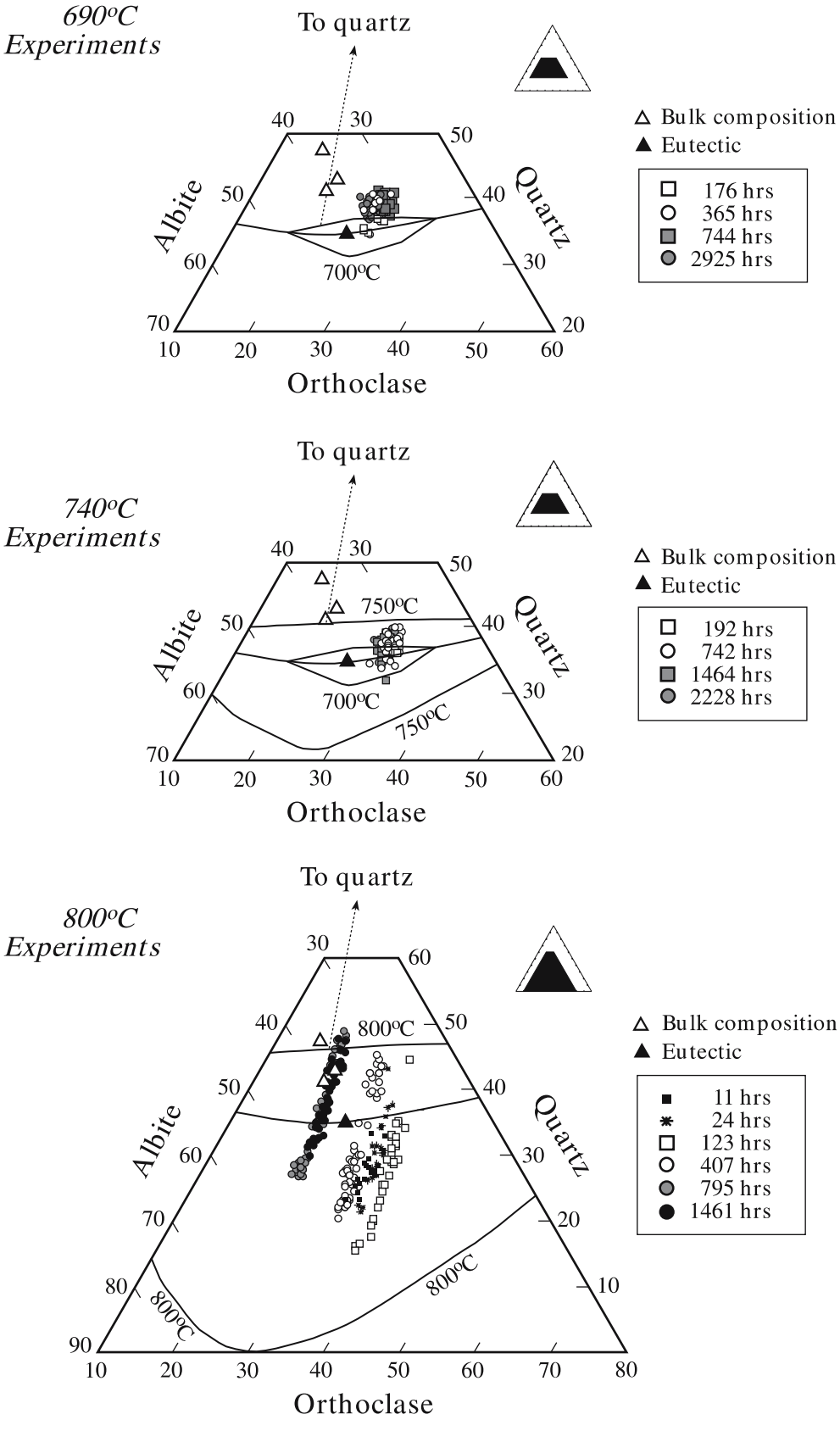

Fig. 10 Weight percentage normative Qtz–Ab–Or composition of experimental glasses as a function of experimental temperature and run duration. The normative composition of the starting bulk composition, and 2 kbar H_2O haplogranite eutectic and 700, 750 and 800°C liquidus isotherms for quartz and feldspar (from Tuttle and Bowen 1958) are also shown

Geological applications and conclusions

Rigorously, this study has applications to the kinetics of melting of quartzo-feldspathic rocks and generation of granite melts, primarily for the case of static melting under H_2O-saturated conditions and with an infinite, though transient, rate of heat supply ("transient" refers to the limited period of time during which the rate of heat supply is infinite for specific cases of crustal melting, e.g. during contact metamorphism associated with intrusion of mantle magmas). For such cases we have shown that melt interconnection throughout the protolith is established at very low degrees of partial melting (e.g. ≤ 5 vol% in the 690°C experiments, Table 2). Thus, crystal grain boundaries are completely occluded with melt films even at the lowest degrees of partial melting. If that occurs in nature also, then once there is a very small volume of melt in a rock, mass transport through that rock by advection of aqueous fluids can no longer occur; from that point on all mass transfer must take place via diffusion through the melt until the rock comes back to conditions of its solidus or below. Experiments of the type presented in this paper are commonly considered as disequilibrium experiments regarding the spatial distribution of melt, the latter being controlled by the location of reactants and the volume change on melting (e.g. Laporte et al. 1997). The fact, nevertheless, is that partial melting under the current experimental conditions produces an interconnected melt network from the beginning of anatexis, which will enable melt segregation and extraction from the very beginning of partial melting (see Sawyer 1994; Brown et al. 1995).

Melting at, or ≈50–70°C above, the solidus produces homogeneous liquids with compositions very close to the haplogranite minimum melt at the appropriate P conditions, which are not in equilibrium with feldspar solid solutions except perhaps right at the interfaces. The rate of melting, though decreases with time (Fig. 3), is relatively fast (≈20–25 vol% partial melting in about 3–4 months, Table 2) and is controlled by the rates of the interface reactions. Equilibration between melt and feldspars, however, might take an extremely long time (see Johannes 1980) due to the absence of mineral recrystallization and sluggish diffusion within the feldspars. Assuming that equilibration takes place via diffusive transport of components through liquid and solid, and using values of alkali diffusivity within feldspars of 10^{-19} to 10^{-20} m^2/s (Giletti and Shanahan 1997) and a mean diameter for restitic feldspars of ≈0.3 mm, we calculate feldspars-melt equilibration times of ≈4,000–40,000 and 7,000–70,000 years using the equation provided by Crank (1975) for diffusion within a sphere or the approximation $x^2 = Dt$, respectively. Increasing the grain size of feldspars to a diameter of 0.5 mm produces an increase of the time of equilibration up to 10,000–100,000 and 20,000–200,000 years. Note that Johannes (1980) calculated, based on his experimental results, equilibration times between micron-sized plagioclase crystals and melt of $\approx 10^{14}$ years at solidus temperatures (660–665°C). Hence, haplogranite minimum melt compositions do not necessarily mean either melting at the minimum temperature or equilibrium melting.

Melting at temperatures well above the minimum (≈100–130°C) is very rapid (≈60–75 vol% partial melting in about 1–2 months, Table 2) and generates disequilibrium, heterogeneous liquids with compositions spread across the central area of the (pseudo-ternary) Qtz–Ab–Or haplogranite space, but none of them on the eutectic. The rate of melting is controlled mostly by diffusivities in the melt, and disequilibrium compositions are controlled by the diffusive transport properties of melt and local equilibrium with neighboring mineral phases. Relict feldspars recrystallize and change entirely their composition rapidly, after only 2 months, whereas melt compositions are still heterogeneous and show variations of ≈10% relative in SiO_2, ≈25% in Na_2O and K_2O, ≈30% in Al_2O_3, and ≈65% in CaO. Calculated diffusivities in H_2O-saturated haplogranite melts at 800°C indicate that under the current experimental conditions, ≈20–30 vol% partial melting of a quartzo-feldspathic protolith and generation of homogeneous equilibrium melts will take place in about 1–10 years, if partial melting and melt homogenization is diffusion in melt-controlled (Acosta-Vigil et al. 2006).

The most important differences between the current experiments and natural melting environments which impede (at least in most cases) the direct application of these results are: the presence of free H_2O in excess, partial melting under differential stress, the occurrence of turbulent and convective flow as mixing mechanisms in melt (in addition to diffusion), and the rate of heat supply.

Brearley and Rubie (1990) partially melted muscovite schist cylinders both under H_2O-saturated and H_2O-undersaturated (no added H_2O) conditions. They found in both cases that melt formed narrow rims in between reactants throughout the entire cores from the beginning of melting, which seemed to constitute a grain boundary network. Melt produced at T closest to the equilibrium melting T were homogeneous, whereas those produced at the highest degrees of T overstepping were heterogeneous. Laporte (1994) have found that a_{H2O} in melt (from H_2O-saturation to dry conditions) does not seem to affect interfacial energies in melt-solid granitic systems and, therefore, does not influence melt distribution. Fluid absent partial melting experiments of pelites indicate that, even under hydrostatic conditions, muscovite melting reactions can create a transient permeability and interconnection of the melt phase that may promote melt segregation (Rushmer 2001). Slower diffusivities associated with a decrease of a_{H2O} in melt (e.g. Watson and Baker 1991) require longer times for melting and melt homogenization, and this effect need to be assessed by investigating diffusivities in melt and kinetics of melting at low a_{H2O}.

Field and experimental studies have shown that melting under non-hydrostatic stress produces a tendency of melt to wet the restite and helps achieving melt

interconnection (Jin et al. 1994; Rushmer 1995; Rutter and Neumann 1995; Rosenberg and Riller 2000; Sawyer 2001; Holyoke and Rushmer 2002). Mechanical (turbulent and convective) mixing during deformation, on the other hand, would tend to decrease melting and homogenization timeframes because it would "refresh" the melt composition in contact with dissolving mineral phases, and would increase the chemical homogeneity of melt. This effect is more difficult to quantify, and perhaps one way to do it would be investigating mineral dissolution in dynamic experiments (e.g. Watson 1982).

The rate of heating is probably much slower in nature than in experiments during the majority of cases associated with the generation of large volumes of crustal granite magmas (i.e. associated with regional metamorphism, see Harris et al. 2000 and references therein). In these cases, the rate of heating constitutes the rate-limiting process during partial melting, increasing greatly the timeframe for melt generation (with respect to kinetic-controlled melting) up to hundreds of thousand years or even million years (Rubie and Brearley 1990). Rubie and Brearley (1990) concluded, however, that even in these cases the rate of melting can be initially controlled by the kinetics of melting if the temperature of the system initially oversteps the equilibrium melting temperature to some extent. In these situations a large amount of melt could be produced in a short time interval. For instance, and following their model, an overstep of 20–100°C would produce 20–50% of melt in 0.2–1 year. Moreover, the equilibration between melt and associated restite is always controlled by kinetics (diffusivities and interface reaction rates), independently of the rate at which the melt is generated. Hence, studies of the kinetics of partial melting are important to understanding the chemistry of natural crustal melts, particularly if we consider (1) the low degrees of partial melting required for achieving melt interconnection in crustal protoliths (see Laporte and Provost 2000, and references therein) necessary for melt segregation (Sawyer 1994; Brown et al. 1995), and (2) the very short melt segregation timeframes reported in some studies of crustal anatectic rocks (e.g. Sawyer 1991; Barbero et al. 1995; Harris et al. 2000). Nevertheless, the present study may have a direct application to some natural melting scenarios, like those associated with partial melting during contact metamorphism. For instance, Holness et al. (2005) have documented the progressive low-pressure, static partial melting of quartzofeldspathic rocks in nature, at the contacts with a mafic plug ≈50 m in diameter. Although the inferred maximum temperatures reached by the rocks (≈850–1,200°C) are significantly higher than in the current experiments, their key observations are comparable to our results. Far from the mafic plug (≈0.4–0.8 m from the contact, calculated maximum temperatures of 850–1,000°C, 0–40 vol% glass), silicate glass forms interconnected films, tens of μm-thick, separating quartz–feldspar and quartz-reacted mica grain pairs. Close to and at the contact (< 0.3 m from the contact, maximum temperatures of ≈1,050–1,200°C, ≈50–60 vol% glass), glass constitutes the matrix of the rock. A large scale chemical communication within the melt network is suggested by the similar composition of glasses at the centers of films in between quartz–feldspar and quartz–mica pairs, in layer-parallel pools, and in veins that cut layering at low angles. Glass compositions in rocks that experienced melting at temperatures closer to the minimum temperature cluster near the minimum melt composition, whereas those from rocks which reached the highest temperatures form linear arrays in Qtz–Ab–Or normative space at high angle with the cotectic line. Finally, the current data have bearing also for understanding and interpreting the chemistry of glass inclusions in partially melted rocks, such as crustal xenoliths in volcanics (e.g. Cesare et al. 1997).

Acknowledgements Support for this research was provided by National Science Foundation grants EAR-990165 and EAR-0124179. The Electron Microprobe Laboratory at the University of Oklahoma was created with US DOE grant DE-FG22-87FE1146 and upgraded with NSF grant EAR-9404658 and support from the University of Oklahoma Office of Research Administration. We are grateful to Bernardo Cesare for comments and Don R Baker and an anonymous referee for thorough reviews which greatly improved a previous version of the manuscript.

References

Acosta-Vigil A, London D, Dewers TA, Morgan GB VI (2002) Dissolution of corundum and andalusite in H_2O-saturated haplogranitic melts at 800°C and 200 MPa: constraints on diffusivities and the generation of peraluminous melts. J Petrol 43:1885–1908

Acosta-Vigil A, London D, Morgan GB VI, Dewers TA (2003) Solubility of excess alumina in hydrous granitic melts in equilibrium with peraluminous minerals at 700–800°C and 200 MPa, and applications of the aluminum saturation index. Contrib Mineral Petrol 146:100–119

Acosta-Vigil A, London D, Morgan GB VI (2005) Contrasting interactions of sodium and potassium with H_2O in haplogranitic liquids and glasses at 200 MPa from hydration-diffusion experiments. Contrib Mineral Petrol 149:276–287

Acosta-Vigil A, London D, Morgan GB VI, Dewers TA (2006) Dissolution of quartz, albite, and orthoclase in H_2O-saturated haplogranitic melts at 800°C and 200 MPa: diffusive transport properties of granitic melts at crustal anatectic conditions. J Petrol 47:231–254

Arzi AA (1978) Fusion kinetics, water pressure, water diffusion and electrical conductivity in melting rock, interrelated. J Petrol 19:153–169

Baker DR (1990) Chemical interdiffusion of dacite and rhyolite: anhydrous measurements at 1 atm and 10 kbar, application of Transition State Theory, and diffusion in zoned magma chambers. Contrib Mineral Petrol 104:407–423

Baker DR (1991) Interdiffusion of hydrous dacitic and rhyolitic melts and the efficacy of rhyolite contamination of dacitic enclaves. Contrib Mineral Petrol 106:462–473

Barbero L, Villaseca C, Rogers G, Brown PE (1995) Geochemical and isotopic disequilibrium in crustal melting: an insight from the anatectic granitoids from Toledo, Spain. J Geophys Res 100:15745–15765

Brearley AJ, Rubie DC (1990) Effects of H_2O on the disequilibrium breakdown of muscovite + quartz. J Petrol 31:925–956

Brown M, Averkin YA, McLellan EL, Sawyer EW (1995) Mechanisms and consequences of melt segregation from crustal protoliths. J Geophys Res 100:15655–15679

Büsch W, Schneider G, Mehnert KR (1974) Initial melting at grain boundaries. Part II: melting in rocks of granodioritic,

quartzdioritic and tonalitic composition. Neues Jahrb Mineral Mh 8:345–370
Cesare B, Salvioli Mariani E, Venturelli G (1997) Crustal anatexis and melt extraction during deformation in the restitic xenoliths at El Joyazo (SE Spain). Mineral Mag 61:15–27
Chakraborty S, Dingwell DB, Rubie DC (1995) Multicomponent diffusion in ternary silicate melts in the system K_2O–Al_2O_3–SiO_2: II. Mechanisms, systematics, and geological applications. Geochim Cosmochim Acta 59:265–277
Cooper AR Jr, Kingery WD (1964) Dissolution in ceramic systems: I, molecular diffusion, natural convection, and forced convection studies of sapphire dissolution in calcium aluminum silicate. J Am Ceram Soc 47:37–43
Crank J (1975) The mathematics of diffusion. Clarendon Press, Oxford
Devineau K, Pichavant M, Villiéras F (2005) Melting kinetics of granite powder aggregates at 1175°C, 1 atm. Eur J Mineral 17:387–398
Donalson CH (1985) The rates of dissolution of olivine, plagioclase, and quartz in basalt melt. Mineral Mag 49:683–693
Giletti BJ, Shanahan TM (1997) Alkali diffusion in plagioclase feldspar. Chem Geol 139:3–20
Hacker B (1990) Amphibolite-facies-to-granulite-facies reactions in experimentally deformed, unpowdered amphibolite. Am Mineral 75:1349–1361
Hammouda T, Pichavant M (1999) Kinetics of melting of fluorphlogopite–quartz pairs at 1 atmosphere. Eur J Mineral 11:637–653
Hammouda T, Pichavant M (2000) Melting of fluorphlogopite-plagioclase pairs at 1 atmosphere. Eur J Mineral 12:315–328
Harris N, Vance D, Ayres M (2000) From sediment to granite: timescales of anatexis in the upper crust. Chem Geol 162:155–167
Holness MB, Dane K, Sides R, Richardson C, Caddick M (2005) Melting and melt segregation in the aureole of the Glenmore Plug, Ardnamurchan. J Met Geol 23:29–43
Holtz F, Behrens H, Dingwell DB, Taylor RP (1992a) Water solubility in aluminosilicate melts of haplogranite composition at 2 kbar. Chem Geol 96:289–302
Holtz F, Johannes W, Pichavant M (1992b) Peraluminous granites: the effect of alumina on melt composition and coexisting minerals. Trans R Soc Edinb Earth Sci 83:409–416
Holtz F, Johannes W, Tamic N, Behrens H (2001) Maximum and minimum water contents of granitic melts generated in the crust: a reevaluation and implications. Lithos 56:1–14
Holyoke CW III, Rushmer T (2002) An experimental study of grain scale melt segregation mechanisms in two common crustal rock types. J Met Geol 20:493–512
Jin Z, Green HW, Zhou Y (1994) Melt topology in partially molten mantle peridotite during ductil deformation. Nature 372:164–167
Johannes W (1978) Melting of plagioclase in the system Ab–An–H_2O and Qz–Ab–An–H_2O at $P_{H2O} = 5$ kbar, an equilibrium problem. Contrib Mineral Petrol 66:295–303
Johannes W (1980) Metastable melting in the granite system Qz–Or–Ab–An–H_2O. Contrib Mineral Petrol 72:73–80
Johannes W (1984) Beginning of melting in the granite system Qz–Or–Ab–An–H_2O. Contrib Mineral Petrol 86:264–273
Johannes W (1985) The significance of experimental studies for the formation of migmatites. In: Ashworth JR (ed) Migmatites. Blackie, Glasgow, pp 36–85
Johannes W (1989) Melting of plagioclase–quartz assemblages at 2 kbar water pressure. Contrib Mineral Petrol 103:270–276
Johannes W, Holtz F (1992) Melting of plagioclase in granite and related systems: composition of coexisting phases and kinetic observations. Trans R Soc Edinb Earth Sci 83:417–422
Jurewicz SR, Watson EB (1985) The distribution of partial melt in a granite system: the application of liquid phase sintering theory. Geochim Cosmochim Acta 49:1109–1121
Kirkpatrick RJ (1981) Kinetics of crystallization of igneous rocks. In: Lasaga AC, Kirkpatrick RJ (eds) Kinetics of geochemical processes. Mineralogical Society of America, Reviews in Mineralogy, vol 8, pp 321–398
Kretz R (1983) Symbols for rock-forming minerals. Am Mineral 68:277–279
van der Laan SR, Wyllie PJ (1993) Experimental interaction of granitic and basaltic magmas and implications for mafic enclaves. J Petrol 34:491–517
Laporte D (1994) Wetting behavior of partial melts during crustal anatexis: the distribution of hydrous silicic melts in polycrystalline aggregates of quartz. Contrib Mineral Petrol 116:486–499
Laporte D, Provost A (2000) The grain-scale distribution of silicate, carbonate and metallosulfide partial melts: a review of theory and experiments. In: Bagdassarov N, Laporte D, Thompson AB (eds) Physics and chemistry of partially molten rocks. Kluwer, Dordrecht, pp 93–140
Laporte D, Watson EB (1995) Experimental and theoretical constraints on melt distribution in crustal sources: the effect of crystalline anisotropy on melt interconnectivity. Chem Geol 124:161–184
Laporte D, Rapaille C, Provost A (1997) Wetting angles, equilibrium melt geometry, and the permeability threshold of partially molten crustal protoliths. In: Bouchez JL, Hutton DHW, Stephens WE (eds) Granite: from segregation of melt to emplacement fabrics. Kluwer, Dordrecht, pp 31–54
Lasaga AC (1981) Rate laws of chemical reactions. In: Lasaga AC, Kirkpatrick RJ (eds) Kinetics of geochemical processes. Mineralogical Society of America, Reviews in Mineralogy, vol 8, pp 1–68
Lasaga AC (1998) Kinetic theory in the earth sciences. Princeton University Press, Princeton, 811 p
Lesher CE (1994) Kinetics of Sr and Nd exchange in silicate liquids: theory, experiments, and applications to uphill diffusion, isotopic equilibration, and irreversible mixing of magmas. J Geophys Res 99:9585–9604
Liang Y, Richter FM, Watson EB (1996) Diffusion in silicate melts: II. Multicomponent diffusion in CaO–Al_2O_3–SiO_2 at 1500°C and 1 GPa. Geochim Cosmochim Acta 60:5021–5035
Linnen RL, Pichavant M, Holtz F (1996) The combined effects of fO_2 and melt composition on SnO_2 solubility and tin diffusivity in haplogranitic melts. Geochim Cosmochim Acta 60:4965–4976
Loomis TP (1983) Compositional zoning of crystals: a record of growth and reaction history. In: Saxena SK (ed) Kinetics and equilibrium in mineral reactions. Advances in physical geochemistry, vol 3. Spriger, Berlin Heidelberg New York, pp 1–60
Lupulescu A, Watson EB (1999) Low melt fraction connectivity of granitic and tonalitic melts in a mafic crustal rock at 800°C and 1 GPa. Contrib Mineral Petrol 134:202–216
Luth WC (1969) The systems $NaAlSi_3O_8$–SiO_2 and $KAlSi_3O_8$–SiO_2 to 20 kb and the relationship between H_2O-content, P_{H2O}, and P_{total} in granitic magmas. Am J Sci 267:325–341
Mehnert KR, Büsch W, Schneider G (1973) Initial melting at grain boundaries of quartz and feldspar in gneisses and granulites. Neues Jahrb Mineral Mh 4:165–183
Morgan GB VI, London D (1996) Optimizing the electron microprobe analysis of hydrous alkali aluminosilicate glasses. Am Mineral 81:1176–1185
Morgan GB VI, London D (1999) Crystallization of the Little Three layered pegmatite-aplite dike, ramona District, California. Contrib Mineral Petrol 136:310–330
Morgan GB VI, London D (2005) The effect of current density on the electron microprobe analysis of alkali aluminosilicate glasses. Am Mineral 90:1131–1138
Mungall JE, Romano C, Dingwell DB (1998) Multicomponent diffusion in the molten system K_2O–Na_2O–Al_2O_3–SiO_2–H_2O. Am Mineral 83:685–699
Nakamura M, Shimakita S (1998) Dissolution origin and syn-entrapment compositional change of melt inclusion in plagioclase. Earth Planet Sci Lett 161:119–133
Pouchou JL, Pichoir F (1985) "PAP" $\varphi(\rho z)$ correction procedure for improved quantitative microanalysis. In: Armstrong JT (ed) Microbeam analysis. San Francisco Press, San Francisco, pp 104–106
Rosenberg CL, Riller U (2000) Partial-melt topology in statically and dynamically recrystallized granite. Geology 28:7–10

Rubie DC, Brearley AJ (1990) A model for rates of disequilibrium melting during metamorphism. In: Ashworth JR, Brown M (eds) High-temperature metamorphism and crustal anatexis. Unwin Hyman, London, pp 57–86

Rushmer T (1995) An experimental deformation study of partially molten amphibolite: application to low-fraction melt segregation. J Geophys Res 100:15681–15696

Rushmer T (1996) Melt segregation in the lower crust: how have experiments helped us? Trans R Soc Edinb Earth Sci 87:73–83

Rushmer T (2001) Volume change during partial melting reactions: implications for melt extraction, melt geochemistry and crustal rheology. Tectonophysics 342:389–405

Rutter E, Neumann D (1995) Experimental deformation of partially molten Westerly granite under fluid-absent conditions with implications for the extraction of granitic magmas. J Geophys Res 100:15697–15715

Sawyer EW (1991) Disequilibrium melting and the rate of melt separation during migmatization of mafic rocks from the Grenville Front, Quebec. J Petrol 32:701–738

Sawyer EW (1994) Melt segregation in the continental crust. Geology 22:1019–1022

Sawyer EW (2001) Melt segregation in the continental crust: distribution and movement of melt in anatectic rocks. J Met Geol 19:291–309

Shaw HR (1963) The four-phase curve sanidine–quartz–liquid–gas between 500 and 4000 bars. Am Mineral 48:883–896

Shaw CSJ (2004) Mechanisms and rates of quartz dissolution in melts in the CMAS (CaO–MgO–Al_2O_3–SiO_2) system. Contrib Mineral Petrol 148:180–200

Taylor JR, Wall VJ (1992) The behaviour of tin in granitoid magmas. Econ Geol 87:403–420

Tsuchiyama A (1985a) Partial melting kinetics of plagioclase–diopside–albite pairs. Contrib Mineral Petrol 91:12–23

Tsuchiyama A (1985b) Dissolution kinetics of plagioclase in the melt of the system diopside–albite–anorthite, and origin of dusty plagioclase in andesite. Contrib Mineral Petrol 89:1–16

Tsuchiyama A, Takahashi E (1983) Melting kinetics of a plagioclase feldspar. Contrib Mineral Petrol 84:345–354

Tuttle OF, Bowen NL (1958) Origin of granite in the light of experimental studies in the system $NaAlSi_3O_8$–$KAlSi_3O_8$–SiO_2–H_2O. Geol Soc Am Mem 74

Wark DA, Stimac JA (1992) Origin of mantled (repakivi) feldspars: experimental evidence of a dissolution- and diffusion-controlled mechanism. Contrib Mineral Petrol 111:345–361

Watson EB (1982) Basalt contamination by continental crust: some experiments and models. Contrib Mineral Petrol 80:73–87

Watson EB (1996) Dissolution, growth and survival of zircons during crustal fusion: kinetics principles, geological models and implications for isotopic inheritance. Trans R Soc Edinb Earth Sci 87:43–56

Watson EB, Baker DR (1991) Chemical diffusion in magmas: an overview of experimental results and geochemical applications. In: Perchuk LL, Kushiro I (eds) Physical chemistry of magmas. Springer, Berlin Heidelberg New York, pp 120–151

Watson EB, Jurewicz SR (1984) Behavior of alkalies during diffusive interaction of granitic xenoliths with basaltic magma. J Geol 92:121–131

Winkler HGF (1974) Petrogenesis of metamorphic rocks, 3rd edn. Springer, Berlin Heidelberg New York

Wolf MB, Wyllie PJ (1995) Liquid segregation parameters from amphibolite dehydration melting experiments. J Geophys Res 100:15611–15622

Wolf MB, London D, Morgan GB VI (1994) Effects of boron on the solubility of cassiterite and tantalite in granitic liquids. Geol Soc Am Abstr Prog 26:450

Zhang Y, Walker D, Lesher CE (1989) Diffusive crystal dissolution. Contrib Mineral Petrol 102:492–513